Sediment size fractionation and focusing in the equatorial Pacific: Effect on ^{230}Th normalization and paleoflux measurements

Citation	Lyle, M., Marcantonio, F., Moore, W. S., Murray, R. W., Huh, C. A., Finney, B. P., ... & Mix, A. C. (2014). Sediment size fractionation and focusing in the equatorial Pacific: Effect on 230Th normalization and paleoflux measurements. Paleoceanography, 29(7), 747-763. doi:10.1002/2014PA002616
DOI	10.1002/2014PA002616
Publisher	John Wiley & Sons, Inc.
Version	Accepted Manuscript
Terms of Use	http://cdss.library.oregonstate.edu/sa-termsofuse

Sediment size fractionation and sediment focusing in the Equatorial Pacific: Effect on ^{230}Th normalization and paleoflux measurements

Working Title: Sediment size fractionation in the equatorial Pacific

Mitchell Lyle[1], mlyle@ocean.tamu.edu

Franco Marcantonio[2], marcantonio@geo.tamu.edu

Willard S. Moore[3], moore@geol.sc.edu

Richard W. Murray[4], rickm@bu.edu

Chih-An Huh[5], huh@earth.sinica.edu.tw

Bruce P. Finney[6], finney@isu.edu

David W. Murray[7], David_Murray@Brown.edu

Alan C. Mix[8], amix@coas.oregonstate.edu

[1]Dept of Oceanography, Texas A&M University, College Station TX 77843

[2]Dept of Geology and Geophysics, Texas A&M University, College Station TX 77843

[3]Dept of Earth and Ocean Sciences,701 Sumter Street, EWS 617, University of South Carolina, Columbia, SC 29208

[4]Dept of Earth & Environment, Boston University, 685 Commonwealth Avenue, Boston, MA 02215

[5]Institute of Earth Science, Academica Sinica, 128 Academia Road, Section 2, Nankang, Taipei 115, Taiwan

[6]Dept of Biological Sciences, Idaho State University, 921 S. 8th Ave, Mail Stop 8007, Pocatello, ID 83209-8007

[7]Dept of Geological Sciences, Brown University, 324 Brook Street, Box 1846, Providence RI 02912,

[8]College of Earth, Ocean, and Atmospheric Sciences, Oregon State University, 104 CEOAS Administration Building, Corvallis, OR 97331-5503

Key Points:

- Weak currents at seafloor preferentially resuspend fine sediments and Th-230
- Carbonate and other coarse fraction lateral transport is overestimated
- Nepheloid layer enriched in Th-230; excess sedimented by high particle flux

Index Terms:

4924 Geochemical tracers, 3022 Marine sediments: processes and transport, 9355 Pacific Ocean, 4912 Biogeochemical cycles, processes, and modeling, 4860 Radioactivity and radioisotopes

Key Words:

Equatorial Pacific, Sediment traps, JGOFS, MANOP, sediment focusing, sediment resuspension

Abstract:

We use flux, dissolution and excess ^{230}Th data from JGOFS and MANOP Site C to assess the extent of sediment focusing in the equatorial Pacific. Measured mass accumulation rates (MAR) from sediment cores were compared to reconstructed MAR by multiplying the particulate rain caught in sediment traps by the ^{230}Th focusing factor and subtracting measured dissolution. $CaCO_3$ MAR is severely overestimated when the ^{230}Th focusing factor correction is large but is estimated correctly when the focusing factor is small. In contrast, Al fluxes in the sediment fine fraction are well matched when the focusing correction is used. Since $CaCO_3$ is primarily a coarse sediment component, we propose that there is significant sorting of fine and coarse sediments during lateral sediment transport by weak currents. Because $CaCO_3$ does not move with ^{230}Th, normalization

typically overcorrects the $CaCO_3$ MAR and because CaCO3 is 80% of the total sediment overestimates lateral sediment flux.

Fluxes of ^{230}Th in particulate rain caught in sediment traps agree with the water column production-sorption model, except within 500 m of the bottom. Near the bottom, ^{230}Th flux measurements are as much as 3 times higher than model predictions. There is also evidence for lateral near-bottom ^{230}Th transport in the bottom nepheloid layer since ^{230}Th fluxes caught by near-bottom sediment traps are higher than predicted by resuspension of surface sediments alone. Resuspension and nepheloid layer transport under weak currents need to be better understood in order to use ^{230}Th within a quantitative model of lateral sediment transport.

1. Introduction:

The equatorial Pacific is a major climate-driven biogeochemical system, large in scale and with a strongly coherent response to climate perturbations. The equatorial Pacific is also a major source of heat flux into the oceans because of the shallow thermocline and upwelling of relatively cold water into the eastern Pacific tropics [Talley et al, 2011]. Upwelling also produces high open ocean productivity, responding to the trade wind field. The strength and seasonal location of the trade winds can thus affect productivity [Murray et al, 1994].

Equatorial Pacific primary production is linked to climate events on multi-annual time scales [Chavez et al., 1999] and apparently has changed as Pleistocene glaciations have

waxed and waned [Lyle et al, 1988; Murray et al, 1995; Paytan et al, 1996; Murray et al, 2000], as well as on longer time scales [Farrell et al., 1995]. The change in production is especially important to understand the extent to which prominent equatorial Pacific CCD cycles are caused by changes in production or dissolution [Farrell et al, 1989, Murray et al, 2000; Anderson et al., 2008]. If production causes the CCD change, the event is linked to changes in nutrient cycles or shallow ocean transport of nutrients, while if dissolution changes the CCD, the event is linked to the abyss and major reorganizations of deep circulation and/or ocean carbon storage.

Changes in paleoproductivity are typically estimated by changes in burial flux of biogenic sediment components [Lyle et al, 1988; Dymond et al, 1992, Murray et al, 1993; Paytan et al., 1996; Murray et al, 2012], and are subject to errors caused by faulty age models, changes in dissolution at the sea floor, and by sediment focusing [Francois et al, 2004]. In the latter case, movement of sediment near the sea floor results in hot spots of higher sediment accumulation (bulk sediment MAR), and there is uncertainty with respect to (a) how much higher MAR are at the hot spot compared to average fluxes, and (b) whether the rate of focusing changes through time and overprints the flux signal.

Using ratios of a biogenic component to another element that is depositing at a relatively constant rate allows sediment focusing to be corrected for. Ratios that have been proposed are Ba/Ti [Murray et al, 2000], ratios to ^{3}He deposition associated with meteoritic debris [Marcantonio et al, 2001], or by normalization to excess ^{230}Th produced from ^{234}U decay in the water column and its subsequent sedimentation to the sea floor

[Bacon, 1984; Francois et al, 2004]. ^{230}Th is assumed to have a constant flux set by its production in the water from ^{234}U. In the simple model, ^{230}Th is immediately adsorbed onto particulate matter and is deposited in sediments. Excess deposition of this unsupported ^{230}Th implies sediment focusing, and the focusing can be normalized away by using a ratio of other sediment components to ^{230}Th.

One hidden assumption of the ^{230}Th normalization methodology is that there is little or no fractionation between high- and low-^{230}Th-containing fractions as the sediment is redistributed [Bacon, 1984]. Since ^{230}Th is known to be enriched in fine-grained sediments with high surface area [Thomson et al, 1993, Kretschmer et al, 2010], there is a possibility that the normalization may produce significant errors if horizontal sediment transport is accompanied by size sorting.

In this paper we gather published and unpublished data from the Joint Global Ocean Flux Study (JGOFS) equatorial Pacific process study and from the nearby Manganese Nodule Project equatorial Pacific study site (MANOP Site C) to evaluate how ^{230}Th is deposited in a pelagic sediment environment with relatively weak bottom currents. We will show that there is significant fractionation of the fine fraction from the coarse fraction that separates ^{230}Th on clays from coarser sediment components. Size fractionation of different sediment components leads to important errors in the sediment balance when using the excess ^{230}Th normalization methodology. We also show via near bottom sediment traps at MANOP Site C that the excess ^{230}Th is primarily redistributed within the nepheloid layer in the lower 500 m of the water column. We propose that sediment

fractionation is likely to be highest in environments of low current activity, in which it is easiest to separate the finest sediment fractions from the remainder of the particulate rain to the sea floor.

2. Setting: biogeochemical studies in the equatorial Pacific

Equatorial Pacific sediments are almost purely biogenic in origin, and are deposited most rapidly at the equatorial divergence where highest upwelling and primary productivity is found. High sedimentation rates are associated with the equatorial region since at least the early Oligocene [van Andel et al, 1975; Moore et al, 2004; Pares and Moore, 2005].

The JGOFS equatorial Pacific process study collected data about the processes that control sediment deposition and biogeochemical cycling across the equatorial region, from 12°S to 9°N. The JGOFS study measured particulate rain by sediment traps [Honjo et al, 1995; Dymond and Collier, 1996], seabed dissolution via pore water profiles and benthic chambers [McManus et al, 1995; Berelson et al, 1997], Holocene burial rates from multicores, and Pleistocene changes in burial via piston coring [Murray et al, 1993; Berelson et al, 1997; Murray et al, 2000]. These sets of measurements make it possible to close the flux equation by measuring both fluxes to the benthic boundary layer from above, and losses from it by dissolution.

The equatorial JGOFS study region is shown in Figure 1a, imaged using the online marine geology application GeoMapApp (http://www.geomapapp.org/). Within the

147 JGOFS equatorial site there is one small seamount 600 m high in the southwest that was
148 avoided in the study. N-S trending abyssal hills are found just W of the sediment trap
149 mooring and west of the core TT013-72PC. They are elevated about 100 m above the
150 valleys between them. There is also an elevated ridge north of the study site that is
151 perhaps 50 m higher than the tops of the abyssal hills. The seafloor has a topographic
152 range between about 4250 and 4400 m, except near the seamount. Because of the thick
153 and uniform sediment cover (400 m based on the 1 seismic line through the area from
154 RC11-10 in 1967, accessed through GeoMapApp), coring was not confined to basins, but
155 also occurred on the flanks of abyssal hills. Francois et al [2004] have assumed that high
156 sediment focusing measured in sediment cores is caused by a bias toward coring basins.
157 However, most of the JGOFS cores were collected about 100 m above a local basin
158 center located about 10 km to the south of the equator.
159
160 MANOP Site C is an important earlier sediment geochemical study in the equatorial
161 Pacific, quantifying pelagic benthic cycling in order to understand how ferromanganese
162 nodules form. Like the JGOFS study sites, all flux parameters were measured so that it is
163 also possible to constrain flux, burial, and dissolution. MANOP Site C is located at 1°N
164 [Figure 1b; Emerson et al., 1982; Murray, 1987; Dymond and Collier, 1988; Walsh et al,
165 1988a,b; Lyle et al, 1988, Berelson et al, 1997]. The site has E-W trending seamounts to
166 the north and parallel E-W abyssal hills to the south, apparently associated with a fracture
167 zone trace. The seamounts rise as high as 3700 m while the abyssal hill in the south rises
168 to about 4100 m. The main basin is about 4450 m deep. The MANOP sediment trap
169 studies differed from those in JGOFS by including near-bottom sediment traps so that

sediment recycling from the sea floor to the lower water column could also be assessed [Walsh et al, 1988a]. MANOP Site C has been important in the understanding of excess ^{230}Th and equatorial Pacific sediment focusing [Marcantonio et al, 2001]. Radiochemical measurements have been made from 3 cores within the study site, so that it is possible to better evaluate the relationship between fluxes and local topography.

3. Data and Methods

Much of the data in this paper has been published elsewhere and is synthesized here, while a few of the data sets have been published only in theses, manuscripts, or are available from data archives. We combine these multiple data sets in order to understand water column particulate fluxes, sediment dissolution at the sea floor, and to understand burial of individual sediment components and excess ^{230}Th.

3.1 Sediment core data

Data used to construct Holocene MAR in Table 2 are from a variety of sources, listed in the table. For most of the cores the chemical, radiochemical, age model and physical properties data needed to construct MAR data were not located in the same papers. For example, for the equatorial Pacific piston core TT13-72PC the radiochemical data are from Marcantonio et al [1996], the $CaCO_3$ and Al data are from Murray et al [2000], and the age model and dry bulk density used are found in Murray et al [2012]. For many of the cores, the radiochemical, age model, and physical properties data are only available from the JGOFS data archive [Berelson and Hammond, 2002; DeMaster, 2002]. Data in

192 Table 2 are reported for the 0-10 ka Holocene section, to average out recent changes in
193 dissolution and to use a time frame more appropriate for a radiocarbon age model in
194 slowly accumulating sediments. We avoided going to the 12 ka boundary because we
195 wanted to avoid any transients associated with the deglaciation.
196
197 Sedimentation rates reported in this paper are either derived from oxygen isotope
198 stratigraphy or from calibrated radiocarbon dates that define the Holocene. For
199 sedimentation rates, we define the sedimentation rate by the thickness of sediment to the
200 date near the base of the Holocene divided by the measured age. We realize that sediment
201 mixing and dissolution can offset radiocarbon ages [Dubois and Prell, 1988; Broecker et
202 al, 1991]. However, the thickness approach has a relatively small error of sedimentation
203 rate under a wide range of dissolution scenarios. Mixing has a tendency to make the
204 radiocarbon age below the mixed layer to be younger than if there were no mixing
205 [Dubois and Prell, 1988]. With a 5 cm mixed layer a sedimentation rate based upon 1
206 radiocarbon date near 10 ka is biased high by about 20-30% versus a sediment with no
207 mixing. Under the condition where all $CaCO_3$ is dissolved in the last 3 kyr as proposed
208 by Berelson et al [1997], a sedimentation rate based upon one fixed age at about 10 ka
209 has about a 10% error, compared to about a 30% error based upon interpolating between
210 two radiocarbon dates below the mixed layer.
211
212 We also report previously unpublished ^{230}Th and ^{232}Th data from core W8402-14GC
213 from MANOP Site C (Supplementary Data Table S1). Bulk sediment chemistry and the
214 age model for the core is from Murray [1987]. Finney and Huh performed radiochemical

215 analyses using the protocol in Huh et al [1990]. A 1-2 g sediment sample was spiked with
216 isotope tracers, then dissolved first with HCl and HF for inorganics, followed by HNO_3
217 and $HC1O_4$ for organics. The samples were dried and then redigested, purified in ion
218 exchange columns, and counted by alpha spectrometry. Since uranium was not
219 determined, a detrital U corrections was made to the excess ^{230Th} by assuming that the
220 uranium content followed the same trend to ^{232}Th as reported for TT013-72PC, the
221 equatorial JGOFS piston core [Winkler et al, 2008]. Initial ^{230}Th was corrected for decay
222 using the Murray [1987] age model.
223

224 ## *3.2 Sediment trap data*

225 Chemical flux data for the JGOFS sediment traps are from Honjo et al [1995]. ^{230}Th
226 fluxes for JGOFS were determined by combining the measurements of ^{230}Th for sediment
227 trap samples reported by Anderson [2002a] with the flux information from Honjo et al
228 [1995] and are reported in Supplemental Table S2. The Anderson [2002a] data were
229 measured from combined splits of individual sediment trap cups. Annual fluxes were
230 calculated by multiplying the concentration of ^{230}Th in the combined samples by the mass
231 collected during that time period, followed by normalizing to a one-year period.
232

233 Unpublished radiochemical data for ^{230}Th and ^{231}Pa for MANOP Site C sediment traps
234 are presented in Table 2, analyzed by alpha spectrometry in Moore's lab in a similar
235 manner to the W8402-14 core data. Details of the analytical method are described in
236 Mahannah [1984] and his data for MANOP Sites H, and M are included in Supplemental
237 Table S3, along with unpublished Site S sediment trap data. Chemical data for the Site C

sediment traps in Table 2 are from Dymond and Collier [1988], with some unpublished additional data for traps that were not included in that paper, supplied by R. Conard (Oregon State University).

Murray [1987] size separated some of the MANOP Site C sediment trap samples and analyzed each fraction for $CaCO_3$, C_{org}, and biogenic silica. The mass of each fraction and its composition are presented in Table 3. Unpublished radiocarbon data from <63μm carbonates from a few of the MANOP Site C sediment traps were made by A. Mix and colleagues and are also included in the supplemental data (Supplemental Table S4).

3.3 Carbonate dissolution measurements

Observed dissolution in the JGOFS transect is from Berelson et al [1997]. These data were measured by benthic chamber incubations at each of the JGOFS equatorial Pacific Sites. They found that modern $CaCO_3$ dissolution is similar to the modern particulate rain, so that little new $CaCO_3$ is accumulating. They also argued that the $CaCO_3$ dissolution rate has increased markedly in the last 3000 years. Stephens and Kadko [1997] and Berelson et al [1997] modeled profiles of U-series radionuclides and $CaCO_3$ to find that an early Holocene dissolution rate of 0.37-0.74 g/cm^2/kyr (0.1 to 0.2 mmol/m^2/day) increased to the modern $CaCO_3$ dissolution rate of 2.1 g/cm^2/kyr (0.58 mmol/m^2/day) at about 3 ka. Stephens and Kadko [1997] suggest that a minor change in carbonate ion concentration in deep water, ~10-15 μM, could drive such dissolution. Because the dissolution rate has not been constant, we have used an average Holocene dissolution rate from 0 to 10 ka of 1.02 g/cm^2/kyr, consistent with the 3-10 ka at a rate of

0.56 g/cm^2/kyr (0.15 mmol/m^2/day) and 0-3 ka at a dissolution rate of 2.1 g/cm^2/kyr (0.58 mmol/m^2/day). Increasing the early Holocene $CaCO_3$ dissolution to the maximum dissolution of 0.2 mmol/m^2/day increases the average dissolution to 1.15 g/cm^2/kyr, while using the minimum estimate of 0.1 mmol/m^2/day yields 0.89 g/cm^2/kyr $CaCO_3$ dissolution.

4. The sedimentation balance: fine fraction (Aluminum) versus coarse fraction ($CaCO_3$)

A model MAR (mass accumulation rate, or mass burial flux) can be calculated by subtracting the measured dissolution from the measured particulate rain to compare to observed MAR. Sediment focusing effects on MAR can be studied by comparing to estimates of MAR with or without focusing ('focus model' and 'no-focus model' MAR, respectively). If there is significant sediment focusing, the focus model should match the observed MAR and the no-focus model MAR should be significantly lower.

The focus model MAR is different from a MAR derived by ^{230}Th normalization because the focus model MAR adds in the hypothesized additional lateral flux while the ^{230}Th normalization attempts to correct for lateral flux by normalizing to a constant production rate of ^{230}Th and by assuming that the incoming lateral flux has the same composition as the vertical particulate rain. In other words, ^{230}Th normalization assumes that there is little or no fractionation of the sediments prior to deposition.

We first assess fine sediment focusing by using Al, since in equatorial Pacific sediments it primarily resides in fine windblown clays, and size fractionation should affect both Al and ^{230}Th during deposition. Furthermore, there is negligible dissolution of refractory clays so that dissolution should not be a factor in its depositional pattern. We then assess coarse sediment focusing using $CaCO_3$, which is primarily found in the coarse fraction of the particulate rain [Murray, 1987]. The $CaCO_3$ focusing must, however, be corrected for dissolution at the sea floor.

4.1 Aluminum MAR and sediment focusing.

We use Al data rather than Ti to represent the fine aluminosilicate fraction despite there being a significant scavenged Al component so that there is higher Al/Ti under regions of high particulate rain [Murray and Leinen, 1996; Dymond et al, 1997]. Cores with Ti data that cover the entire Holocene interval are too few to use for an assessment. Since Al is particle reactive, it should still track the fine fraction adequately.

We have Al data along with ^{230}Th data from the complete Holocene section for 5 cores (Table 1) but unfortunately have Holocene Ti data for only 2 cores [Murray et al, 2000, 2012]. XRF-derived Ti data from MANOP Site C cores [Murray, 1987] is uncalibrated and likely too high. Core-top Ti data is available for many other cores [Murray and Leinen, 1996], but because of the higher $CaCO_3$ dissolution within the last 3000 yr [Stephens and Kadko, 1997], the topmost sediments are enriched in the refractory elements, including ^{230}Th and Ti. If the average sedimentation rate is applied with only the uppermost sample, the resulting MAR is artificially high. Ti flux in particulate rain is

304 available for JGOFS sediment traps [Dymond et al, 1997], but was not measured at the
305 MANOP Site C sediment trap deployment.
306
307 The Al MAR distribution can be explained by sediment focusing. Figure 2 (Table 1)
308 illustrates that Al focusing in the equatorial Pacific sediments (i.e., the ratio of Al MAR
309 in the sediments to the Al rain from sediment traps) is similar to the degree of sediment
310 focusing predicted by the ^{230}Th-estimated focusing factor where we have data, at the
311 JGOFS 2°S and equatorial study sites [TT013 18 and 72 PC, Murray et al, 2000; 2012;
312 Winckler et al, 2008], and MANOP Site C [W8402-14GC, BNTH-18GC, and BNTH-
313 25GC; Marcantonio et al, 2001; Murray, 1987].
314
315 At MANOP Site C we use the two year average of Al rain in the 3495 m trap in year 1
316 and the 2908 m trap in year 2 (2.41 mg/cm^2/kyr; supplemental data table S1) rather than
317 the published Site C Al flux [5.41 mg/cm^2/kyr; Dymond and Lyle, 1994) because that Al
318 flux was based on a sediment trap at 4170 m, within the sedimentary rebound zone
319 [Walsh et al, 1988a] and contains Al rain recycled from the sea floor, as discussed later.
320 If the Dymond and Lyle [1994] Al flux at MANOP Site C is used, all of the measured Al
321 MAR are less than the particulate Al rain, but if the revised value is used, the degree to
322 which Al is focused is matched by ^{230}Th. High ^{230}Th deposition is correlated with high Al
323 deposition, supporting the assumption that both elements are found in the same sediment
324 fraction, probably associated with fine sediments. The 20% higher Al focusing than ^{230}Th
325 focusing is best explained by more variability of Al particulate rain where the average is
326 not well-resolved with only 2 years of data.

The 3 cores at MANOP Site C at 1°N have focusing factors that range from 0.94 to 1.48 (Table 1), and allow some exploration of the pattern of sediment focusing. The lowest focusing factor (0.94) is found in BNTH-18GC, next to the NE seamount (Figure 1b). Of the other 2 cores, W8402A-14GC is at the top of a sedimented ridge and has a focusing factor of 1.37, while BNTH-25GC is in a basin 114 m deeper than 14GC and has a focusing factor of 1.48. Distance away from the seamounts and the higher currents there appear to be more important factors to influence focusing rather than position at the top or the bottom of the subdued topography.

Because of the paucity of particulate rain data available for the equatorial Pacific, only basic conclusions can be made. Nevertheless, ^{230}Th-estimated focusing can explain the distribution of MAR observed in the sedimentary fine fraction as represented by Al.

4.2 $CaCO_3$ MAR and sediment focusing.

Studying $CaCO_3$ MAR in order to understand movement of the coarse sediment fraction is more difficult than using Al MAR to study the fine fraction because there is $CaCO_3$ dissolution at the sea floor. The dissolution correction has 2 difficulties—first, direct measurements of $CaCO_3$ dissolution are hard and the errors can cause a large uncertainty in estimating $CaCO_3$ MAR by subtracting $CaCO_3$ rain from dissolution. Of equal importance, large changes in $CaCO_3$ dissolution have occurred in the Holocene [Stephens and Kadko, 1997; Berelson et al, 1997]. Despite the change, averaging the $CaCO_3$ sediment concentration and the dissolution rate over the Holocene makes it possible to compare an expected value calculated from the particulate rain and dissolution to an

observed MAR, which is measured over 5-10 kyr time intervals in slowly accumulating sediments. As shown below, the laterally transported coarse fraction (as tracked by $CaCO_3$ MAR) can be significantly overestimated using the ^{230}Th normalization, making the ^{230}Th normalized $CaCO_3$ MAR too low.

The MAR calculation based on $CaCO_3$ particulate rain and dissolution assumes that the modern $CaCO_3$ rain measured in the equatorial Pacific sediment traps is similar to the average Holocene value. There is very little data to evaluate the stability of particulate rain since only low-flux subtropical gyres have been monitored on a long-term basis (e.g., Hawaii Ocean Time Series, http://hahana.soest.hawaii.edu/hot/hot_jgofs.html). However, The MANOP Site C sediment traps were deployed during the strong 1982-83 el Niño and the recovery year following it [Dymond and Collier, 1988; Table 2], which should represent an extreme range of difference in biogenic rain. There was a maximum 40% difference of $CaCO_3$ rain over the two years, which we suggest is near the maximum variability of $CaCO_3$ rain that might be found under relatively constant climate conditions. Furthermore, $CaCO_3$ particulate rain at MANOP Site C (1°N) in the 1982-1984 period is between the $CaCO_3$ particulate rain measured by JGOFS at the equator and 2°N in 1992 (Honjo et al, 1995), as expected if the $CaCO_3$ rain is near the long-term average.

We estimated Holocene $CaCO_3$ MAR in three ways—(1) *the focused model $CaCO_3$ MAR estimate*, by multiplying the $CaCO_3$ rain by the ^{230}Th focusing factor and then subtracting $CaCO_3$ dissolution, (2) *the no-focus model $CaCO_3$ MAR*, by subtracting average

373 Holocene dissolution from the measured particulate $CaCO_3$ rain without any adjustment
374 for focusing, and (3) *the observed $CaCO_3$ MAR* calculated by using measured age-model-
375 derived sedimentation rates, bulk density, and $CaCO_3$ % in Holocene sediments (Table
376 1). Table 1 lists the source of dating and $CaCO_3$ content. Bulk density was estimated
377 either by using the $CaCO_3$ method [Murray, 1987], or by using porosity data [Berelson
378 and Hammond, 2002] and assuming a sediment grain density of 2.7 g/cm^3.

379

380 For both the no-focus and focused model $CaCO_3$ MAR estimates, we have assumed that
381 $CaCO_3$ dissolution rate is approximately constant across the JGOFS latitudinal transect,
382 as suggested by Berelson et al [1997]. All cores were collected at similar water depths, so
383 should experience similar dissolution rates. We use $CaCO_3$ records from 0-10 ka where
384 possible, to approach the entire length of the Holocene but to avoid the end of the
385 deglaciation.

386

387 The focused $CaCO_3$ MAR model can be restated as

388 (1) $MAR_{CaCO3} = F*R_{CaCO3} - D_{CaCO3}$

389 where F is the ^{230}Th focusing factor [excess ^{230}Th burial over production; Suman and
390 Bacon, 1989], R is the rain rate of $CaCO_3$, and D is the dissolution rate of $CaCO_3$. Since
391 the $CaCO_3$ dissolution rate is nearly constant and independent of particulate rain, and if
392 the particulate rain is not fractionated, high $CaCO_3$ MAR should occur at the sea floor
393 where there is high sediment focusing.

394

395 Focused model $CaCO_3$ MARs are systematically higher than observed when focusing
396 factors are >1.3, while the no-focus flux model MAR more closely matches the observed
397 $CaCO_3$ MAR at all focusing factors (Figure 3). The no-focus model $CaCO_3$ MAR is
398 somewhat flatter than the observed $CaCO_3$ MAR, however. There is relatively small
399 variation in particulate $CaCO_3$ rain between 5°N and 5°S (<35% difference from the peak
400 equatorial value along the transect; Table 1), and the model assumes that $CaCO_3$
401 dissolution is constant. Dissolution may be somewhat anti-correlated with sedimentation
402 rate, or there may be a minor amount of sediment focusing of $CaCO_3$, [Lyle et al, 2005;
403 Tominaga et al, 2011]. We will further explore fractionation of $CaCO_3$ from Al and ^{230}Th
404 using sediment trap data in section 5.
405
406 Could some systematic error make measured sedimentation rates lower where sediments
407 are highly focused in order to insert a low bias to the observed $CaCO_3$ MAR? Core
408 deformation during collection may affect core length, while bioturbation and interface
409 dissolution at the benthic boundary affect radiocarbon age [e.g., Keir and Michel, 1993]
410 and could cause systematic sedimentation rate errors. However, such errors cause
411 positively correlated changes in both measured $CaCO_3$ MAR and the ^{230}Th focusing
412 factor, so they would not affect the offsets. If the $CaCO_3$ MAR is low because of an error
413 that lowers the sedimentation rate, the ^{230}Th focusing factor will also be lower than the
414 actual value, and the difference between measured and focused estimate of $CaCO_3$ MAR
415 will also be reduced. Whenever the focusing factor is above 1, it is impossible to cause
416 the offset between observed $CaCO_3$ MAR and the focused $CaCO_3$ MAR estimate by a
417 sedimentation rate error alone.

4.2 Why do $CaCO_3$ and Al behave differently? The size fractionation hypothesis

Murray [1987, Table 3] shows that most of the $CaCO_3$ rain is in the coarse fraction. He performed a size analysis of both $CaCO_3$ and opal in sediment traps at MANOP Site C to determine the relative contribution of phytoplankton and zooplankton to the biogenic rain. Murray (1987) sieved different size fractions and measured the Ca and biogenic Si contents in each to determine carbonate and opal %. The residual fraction listed in Table 3 is >95% organic carbon. Between 68-78% of the total mass of $CaCO_3$ resides in size fractions greater than 38μm, while 45-50% is >150μm. The $CaCO_3$ rain largely consists of silt to sand-sized foraminiferal tests, plus some $CaCO_3$ incorporated into well-packed aggregates resistant to breakup by sieving. These large sediment grains are not susceptible to resuspension.

The <38μm sieve fraction also includes relatively large silt sizes that may not travel far under weak current conditions. The spherical Stokes settling rate for $CaCO_3$ particles between 20 and 38μ is between 32 and 115 m/d. Mitchell and Huthnance [2013] reported net near-bottom currents of 1-2 cm/s moving SE at MANOP Site C during the trap deployments (transport of 0.9-1.7 km/day). Further evidence of low current activity around MANOP Site C comes from bottom photography during a deep-tow survey of Site C in 1980 (RAMA-1), one year after a 1979 coring campaign that collected a grid of transponder-navigated box-cores (K7905). The box core (figure 4a) has a roughly triangular frame that leaves an imprint on the bottom when it lands. Still visible after a year (Figure 4b), the outline of the box core frame is distinct, indicating that there was

441 little meaningful current activity that impacted the bottom over that year. While evidence
442 exists for typically low currents, the current meter data discussed in Section 6 also show
443 periods of high activity that influenced horizontal transport and help to test hypotheses of
444 sediment rebound.
445
446 The aluminosilicate fraction captured in the sediment traps consists of fine grains since
447 essentially all clays in the central Pacific is windblown dust with grain sizes <4μm
448 [Chuey et al, 1987]. The aluminosilicate particles are scavenged by larger aggregates and
449 released when aggregates break down and re-form in the water column. The time that
450 these particles reside in the water column depends upon the time taken for large particles
451 to aggregate, probably controlled by biological activity [McCave, 1984]. Since $CaCO_3$ is
452 primarily coarse-grained, it is very likely that sediment sorting near the bottom could
453 fractionate clays (and ^{230}Th) from carbonate in the weak currents found around MANOP
454 Site C.
455

456 ## 5. MANOP Site C Sediment trap ^{230}Th fluxes, $CaCO_3$
457 ## fluxes and sediment rebound in the nepheloid layer

458 Sediment trap data exists for ^{230}Th and other particulate fluxes in the equatorial Pacific
459 fromJGOFS [Honjo et al, 1995; Dymond and Collier, 1996; Anderson, 2002] and from
460 MANOP [Dymond and Collier, 1988; Table 2]. As part of the two-year trap deployment
461 at MANOP Site C, sediment traps were moored between 1 and 3 km below the surface

462 and additional traps were moored within the sediment resuspension zone between ~4 km
463 and the bottom at 4.45 km [Walsh et al, 1988a].
464

465 *5.1 Uranium-series sediment trap fluxes and rebound*

466 Two flux zones are apparent, a water column zone, and a near-bottom zone (Figure 5a,
467 Table 2, Supplementary Table S2). Fluxes of ^{230}Th measured in both the JGOFS and
468 MANOP sediment traps >500 m above the sea floor fit a model of water column ^{230}Th
469 production and efficient particle scavenging to carry the ^{230}Th flux to the bottom,
470 following Krishnaswami [1976]. There is no clear sign of enhanced ^{230}Th particulate flux
471 near the equator by boundary scavenging in the water column [Broecker, 2008]. In
472 contrast, there are high fluxes of ^{230}Th in sediment traps in the lower 500 m of the water
473 column (Table 2) associated with higher sediment fluxes rebounding from the bottom
474 [Walsh et al, 1988a].
475
476 Walsh et al [1988a] described the near-bottom cycling of sediment as rebound because
477 the recycled flux caught in near-bottom traps was intermediate in composition between
478 that of surface sediments and that of the particulate rain. The additional flux caught in
479 sediment traps has higher biogenic opal and C_{org} contents than the surface sediments. If
480 the additional flux is modeled as an addition of surface sediments alone, the opal and C_{org}
481 fluxes are underestimated by >20%. In contrast, the $CaCO_3$ flux is overestimated,
482 suggesting that the coarse $CaCO_3$ fraction does not rebound as efficiently (Walsh et al,
483 1988a).
484

485 Particle rebound is problematic because there usually is not sufficient energy to lift
486 sediment 'fluff' off the bottom to as high as 500 m above the sea floor. For this reason, it
487 has been argued that seamounts and currents around them might provide either the lift or
488 the sediment source (Turnewitsch et al, 2013) or that there is significant lateral transport
489 (e.g., Baldwin et al, 1998). The source of particles will be investigated further in Section
490 6.
491
492 Clearly, ^{230}Th fluxes near the bottom are also being cycled back to the water column
493 before burial. Using a sediment-mixing model like that of Walsh et al [1988a], Al can be
494 used to estimate the expected recycled ^{230}Th flux. A rebound ^{230}Th/Al is calculated by
495 extrapolating the water column ^{230}Th flux to the depth of the sea floor and dividing by
496 the water column flux of Al, measured above the rebound zone. Multiplying the excess
497 flux of Al caught by the traps by this ratio produces an excess ^{230}Th flux that should have
498 been caught by the traps. The 'rebound' model of ^{230}Th flux enrichment underestimates
499 the measured ^{230}Th flux enrichment (Table 3) and there appears to be additional ^{230}Th
500 flux added in the lower water column.
501
502 The ^{230}Th flux enrichment relative to surface sediments can also be deduced by
503 comparing ^{230}Th/Al in the sediment traps vs that of the sediments at Site C (Table 2).
504 The average Site C ^{230}Th/Al in sediment traps below 3000 m is 26% higher than the
505 surface sediments, 5.24 dpm/ng Al versus a ratio of 4.15 in surface sediments (average
506 for the uppermost samples of BNTH-18GC, -25GC, and W84-14GC). The higher
507 ^{230}Th/Al in sediment traps may reflect addition of ^{230}Th-rich particles that are drifting in

508 the nepheloid layer, or it may represent an enrichment of ^{230}Th in lower water column
509 particulates caused by loss from the sediments when surfaces of labile particles dissolve
510 before burial. Roughly 2/3 of the $CaCO_3$ dissolves before burial, as well as 90% of the
511 biogenic opal and 99% of the C_{org} at MANOP Site C [Dymond and Lyle, 1994]; much of
512 the ^{230}Th released by the dissolving particulate matter would immediately sorb to the
513 remaining sediment surfaces, but a small fraction could diffuse back to the water column.

514 ## *5.2 $CaCO_3$ sediment trap fluxes and rebound*

515 Resuspension preferentially sends small grains back to the water column. $CaCO_3$ fluxes
516 caught in the near-bottom traps at Site C are lower than expected unless coarse $CaCO_3$
517 remains at the bottom. ^{230}Th ratios to $CaCO_3$ in the traps can be used to indicate the
518 relative sorting (Figure 5b). We calculate an expected value of ^{230}Th:$CaCO_3$ for
519 rebounded sediments by extrapolating both the ^{230}Th flux and the water column
520 dissolution of $CaCO_3$ [Walsh et al.,1988b] to the water depth of the bottom (4450 m. The
521 expected ^{230}Th:$CaCO_3$ ratio, in dpm/g $CaCO_3$, is 5.71. The measured ^{230}Th:$CaCO_3$ ratio in
522 near bottom traps is as high as 16.71 in the traps set closest to the bottom, indicating a
523 major deficit of $CaCO_3$. A ^{230}Th-rich fraction is about 3 times more likely to be
524 resuspended than the $CaCO_3$-rich fraction. Nevertheless, there is still evidence of $CaCO_3$
525 resuspension (Table 3). The flux of $CaCO_3$ captured in sediment traps within 500 m of
526 the bottom is higher than fluxes from above the resuspension zone, indicating that 8-20%
527 of the $CaCO_3$ caught by sediment traps in the resuspension zone is recycled from the
528 bottom.
529

Radiocarbon dating of the <63μm $CaCO_3$ fraction from the MANOP Site C sediment trap set (Supplemental Table S4) indicates sediment resuspension. Old $CaCO_3$ was caught in the sediment trap at 4295 m ($\Delta^{14}C$ of -142, Supplemental table S4). If the resuspended material has the same age as surface sediments ($\Delta^{14}C$ of -440) the 4295 m sediment trap received 46% resuspended $CaCO_3$ as compared to 20% resuspended $CaCO_3$ from the excess $CaCO_3$ flux.

The radiocarbon-estimated resuspended flux should only be compared to the <63μm $CaCO_3$ caught by the traps since only the <63μm $CaCO_3$ fraction from the sediment traps was ^{14}C dated. Foraminifera that make up the coarse fraction were not dated because they should have modern ages. The <63μm $CaCO_3$ is only 30-40% of the total $CaCO_3$ rain [Table 2; Murray, 1987]. If only the <63μm $CaCO_3$ fraction of the sediments was resuspended, a 20% addition of fine $CaCO_3$ from surface sediments would be equal to ~ 40% of the radiocarbon-dated fraction. The 46% level of fine $CaCO_3$ from ^{14}C is also similar to the Al resuspension estimate in the same sediment trap (57%), and indicates that the fine $CaCO_3$ fraction is recycled back to the water column at a similar rate as other fine sediment fractions, but that coarse $CaCO_3$ remains at the sea floor.

The data from MANOP Site C indicates that sediment focusing preferentially affects the fine fraction and leaves the coarser component of sediments in place where they have fallen to the bottom.

6. What causes excess flux in the near-bottom sediment traps?

In the relatively weak currents found at MANOP Site C and much of the equatorial Pacific there is a separation of coarse from fine sediments and the fine fraction is preferentially resuspended and possibly transported. Most of the coarse fraction, in particular $CaCO_3$ in the equatorial Pacific, remains where it has fallen to the bottom and is not focused strongly. Measurements in near-bottom sediment traps indicate that 8-20% of the $CaCO_3$ is resuspended, versus 50-60% of the Al.

Seasonal sediment trap data combined with current meter data at MANOP Site C provides insight into how the sediment is resuspended and redeposited. Current direction and velocity data can be compared with excess flux caught in the sediment traps to better understand sources of the resuspended particulates. .

6.1 Sediment resuspension and dispersion in the equatorial Pacific

Although bottom nepheloid layers often extend 500-1500 m above the bottom [McCave, 2009], they are most common in the Atlantic and thought to form where sufficiently strong currents impinge the bottom to lift particles and then stream laterally for long distances [McCave, 1986]. In the Pacific Ocean, such strong currents are not thought to be present in the interior and ocean margin sources of sediment are thousands of km away. Turnewitsch et al [2013] have suggested that tidal activity interacting with

seamounts may provide the lift as well as be the source for resuspended sediments. If they are correct, maximum resuspension at MANOP Site C should associate with high current activity believed to be from NE-SW, based upon sedimentary erosional features in the vicinity identified by Mitchell and Huthnance [2013]. Southwest flowing bottom water in the central equatorial Pacific is consistent with evidence for a gyre of Circumpolar Deep Water flowing eastward at about 15°N, turning south on the west flank of the East Pacific Rise and flowing westward at the equator [Johnson and Toole, 1993].

In the MANOP Site C region, high topography surrounds the sediment trap moorings (Figure 1b). A small seamount to the north is about 750 m above the level of the basin (4450 m), while to the east is a larger seamount about 850 m above basin level. To the south is a sediment-covered ridge with a few outcrops that reaches about 350 m above the basin floor. If currents are generated around the relief, there should be high sediment rebound when currents are high, especially when they flow in a southerly direction.

6.2 MANOP Site C currents and near-bottom sediment fluxes

Near-bottom current meter data from the 1982-1985 MANOP Site C sediment trap deployments are available on line from the Oregon State University Buoy Group (http://kepler.oce.orst.edu/quick/archive.htm) and were first discussed in Mitchell and Huthnance (2013). The pertinent data are shown in figure 6, which joins data from a current meter 20 meters above bottom (mab) on the MANOP C-1 mooring (4450 m current meter depth) and a current meter 55 mab on the C-3 mooring (4395 m depth to meter) to form an 866 day near bottom current record (from 12 Dec 1982 to 26 April

1985), The current meter records starts near the peak of the 1982-83 ENSO event and extend nearly 2 years beyond the end of the ENSO. The ENSO high SST anomaly ended at about July 15 1982 (day 561 from the beginning of 1982; Dymond and Collier, 1988).

Most of the currents in the MANOP Site C records vary in long period cycles, and not with tides (Figure 6). Diurnal and semi-diurnal currents have a maximum amplitude of ~5 cm/s, while maximum current velocity for the whole record is 24.66 cm/s. Multiday variability is typical of the record, with periodicity of 17 and 11 days during the 1982-83 ENSO that changes to 37-day and 17-day periodicity after mid July 1983. High current velocities typically lasted for many days and are associated with a currents flowing to the SW (205-220°), roughly aligning with the gap between the seamounts to the north of the moorings (Figure 1b). Less frequently, relatively high current speeds were associated with currents traveling in the converse direction, to the NE.

If increased flux in sediment traps resulted from resuspension from the nearby seamounts, there should be a correlation between sediment rebound flux caught in the bottom traps and time intervals with high current velocity, especially from the NE to the SW. The highest current speeds were between days 658 to 736 (Figure 6c), about 3 months after the disappearance of the ENSO SST anomaly. The sediment trap cup 5 period of the C-1 and C-2 moorings (day 652 to 780, Table 2) is the equivalent sediment trap collection period.

618 The lower sediment traps do collect higher mass flux than traps located above the
619 seamount level within the time of high currents. For example, the cup 5 period in traps >4
620 km deep collected 30-70% more total mass flux than the 3495 m cup 5. In addition, in the
621 4170 m trap the ^{230}Th mass flux was about 20% higher and the Al flux 35% higher than
622 the average annual flux at that depth over the full deployment. The data thus support a
623 sediment injection into the lower water column during the high current period possibly
624 from the seamounts.
625
626 In contrast, the highest total mass flux as well as fluxes of Al and ^{230}Th come with the
627 highest vertical mass flux period, in the cup 3 collection period of mooring C-3 (days 886
628 to 986 in the 4390 m sediment trap). During this time period currents were generally
629 low—current speeds only topped 10 cm/sec for a few hours in the 100 days. The typical
630 current direction was toward the NE, even during all but one of the higher current
631 intervals. The median speed during the cup 3 period, 4.6 cm/s, is 10% less than the
632 median for the total record.
633
634 High fine-particle fluxes associated with high vertical flux probably results from large
635 particles sweeping up fines as they fall through the water column [McCave, 1984]. Since
636 the excess Al and ^{230}Th flux is caught within the bottom nepheloid layer, the high fluxes
637 apparently strip out a standing stock of fine particles in the lower water column.
638 Depending on the residence time of these particles within the nepheloid layer they may
639 scavenge additional ^{230}Th from the water column as they reside there. Such behavior is
640 seen in the lower water column in the Panama Basin associated presumably with higher

particle concentrations (Singh et al, 2013). There is a significant deficit of ^{230}Th in the lower depths of the basin below that predicted by an equilibrium-scavenging model.

In the deepest MANOP Site C sediment traps, more ^{230}Th is systematically caught than expected based upon surface sediment resuspension (Table 4). In the 4390 m trap from the C-3 mooring, there is 80 dpm/m^2/yr more ^{230}Th than predicted by the excess Al recycled to the trap. This excess is ~70% of the vertical flux of ^{230}Th to the sediments. If sorption of ^{230}Th to particles depends on the time the particle resides in the water column, potentially one could calculate an average residence time of particles in the nepheloid layer. In any case, a ^{230}Th-rich fine fraction traveling within the bottom nepheloid layer potentially can explain why it is very difficult to identify any cores in the tropical Pacific with a focusing factor less than one.

6.3 Current velocity, particle sorting, and sediment focusing

Within the abyssal oceans there appears to be a spectrum of fine-fraction (and ^{230}Th) sorting depending on the typical current regimes. With higher typical currents, coarse sediments are more poorly fractionated from fine sediments. McGee et al [2010], for example, found little fractionation of either ^{230}Th or ^{3}He from extraterrestrial dust on the Blake Ridge, under a regime where there is high variability of lateral fluxes and relatively high current activity.

Marcantonio et al [Marcantonio, F., M. Lyle, R. Ibrahim, Particle sorting during sediment redistribution processes and the effect on ^{230}Th-normalized mass accumulation rates, submitted to Geophysical Research Letters, 2014] examined paired sites on the Cocos

and Carnegie Ridges, where moderate current activity transports sediments off the ridge crests and into the basins below. They found that the sand-sized fraction MAR, essentially all foraminifera, was nearly the same for each pair of sites if a radiocarbon age model was used. When ^{230}Th normalization was used the normalized sand fluxes were systematically much lower in the basin sites, indicating preferential movement of a ^{230}Th-rich fraction. They proposed that the sorting is actually greatest when current velocities are relatively low, leaving the coarse fraction in place and transporting fine ^{230}Th-rich grains downslope. We concur, and also suggest that long-distance transport in within the bottom nepheloid layer may further enrich the fine sediment in ^{230}Th, since additional exposure to seawater will allow the fine particle to capture additional ^{230}Th as it travels. We speculate that higher apparent sediment focusing near the equator may be because of better capture of the nepheloid ^{230}Th by higher vertical particle fluxes. It is clear from cores on top of hills versus in the basin at MANOP Site C that topography has a small effect on focusing factor.

7. Conclusions

Comparison between near-bottom sediment traps and surface sediment data in the equatorial Pacific indicate that the fine fraction of abyssal sediments is involved in resuspension in the nepheloid layer and is preferentially sedimented out by high vertical flux. The fine fraction is enriched in ^{230}Th and will preferentially accumulate where there is high vertical particulate rain and in quiet areas where the fine sediment fraction can settle out. Fluxes of coarse sediment components, like $CaCO_3$, are better estimated by direct measurement of MAR than by ^{230}Th normalization .

Two processes thus control the sedimentation of fine sediment components—first a buildup of an excess concentration in the nepheloid layer followed by a rainout when or where a high vertical flux of large particles occurs. The rainout of fine sediments is documented by the excess ^{230}Th and Al fluxes at the equator. In addition, enrichment of Al relative to Ti (Murray and Leinen, 1996; Dymond et al, 1997) suggests that scavenging plays an important role to enrich certain elements within the nepheloid layer. However, it is still unclear how the bottom nepheloid layer is maintained in low current environments, why it is enriched in biogenic sediment components, and to what extent it fines within the bottom nepheloid layer travel horizontally. Further fieldwork is needed to clarify these important issues.

Acknowledgments

The excellent fieldwork and data collection more than two decades ago by our JGOFS and MANOP colleagues provide the basis for this paper. Unfortunately, no equatorial Pacific particle flux experiments have been undertaken since JGOFS. We thank David McGee and an anonymous reviewer for constructive reviews. NSF grants OCE-0851056 and OCE-0962184 provided support for the analysis and writing.

References

Anderson, R.F. (2002a) Radionuclides, moored sediment trap samples. United States JGOFS Data Server. Woods Hole Oceanographic Institution, USA: U.S. JGOFS

Data Management Office, iPub. Accessed: 2013. http://usjgofs.whoi.edu/jg/dir/jgofs/eqpac/tt013/

Anderson, R.F. (2002b) Radionuclides, sediment cores, EqPac/TT013. United States JGOFS Data Server. Woods Hole Oceanographic Institution, USA: U.S. JGOFS Data Management Office, iPub. Accessed: 2013. http://usjgofs.whoi.edu/jg/dir/jgofs/eqpac/tt013/

Anderson, R. F., M. Q. Fleisher, Y. Lao, and G. Winckler (2008), Modern $CaCO_3$ preservation in equatorial Pacific sediments in the context of late Pleistocene glacial cycles, Marine Chemistry, 111, 30-46.

Bacon, M. P. (1984), Glacial to interglacial changes in carbonate and clay sedimentation in the Atlantic Ocean estimated from 230Th measurements, Isotope Geoscience, 2, 97-111.

Baldwin, R. J., R. C. Glatts, and K. L Smith jr. (1998), Particulate matter fluxes into the benthic boundary layer at a long time series station in the abyssal NE Pacific: composition and fluxes, *Deep Sea Research II*, *45*, 643-665.

Berelson, W. M., R.F. Anderson, J. Dymond, D.J. DeMaster, D.E. Hammond, R. Collier, S. Honjo, M. Leinen, J. McManus, R. Pope, C. Smith, M. Stephens, (1997), Biogenic budgets of particle rain, benthic remineralization and sediment accumulation in the equatorial Pacific, Deep Sea Research II, 44(9-10), 2251-2282.

Berelson, W., D. Hammond (2002) Porosity and pore water nutrient chemistries, sediment cores, EqPac/Cruise TT013, Benthic survey. United States JGOFS Data Server. Woods Hole Oceanographic Institution, USA: U.S. JGOFS Data

731 Management Office, iPub. Accessed: 2013.
732 http://usjgofs.whoi.edu/jg/dir/jgofs/eqpac/tt013/

733 Broecker, W. S., M. Klas, and E. Clark (1991), The influence of CaCO3 dissolution on
734 core top radiocarbon ages for deep-sea sediments, Paleoceanography, 6(5), 593-
735 608.

736 Broecker, W. (2008), Excess sediment ^{230}Th: transport along the sea floor or enhanced
737 water column scavenging?, *Global Biogeochemical Cycles*, *22*, GB1006, 4pp.

738 Chavez, F., P. G. Strutton, G. Friederich, R. A. Feely, G. C. Feldman, D. G. Foley, and
739 M. J. McPhaden (1999), Biological and chemical response of the equatorial
740 Pacific Ocean to the 1997-1998 El Niño, Science, 286,2126-2131.

741 Chuey, J. M., D. K. Rea, and N. G. Pisias (1987), Late Pleistocene paleoclimatology of
742 the central equatorial Pacific: a quantitative record of eolian and carbonate
743 deposition, *Quaternary Research*, *28*, 323-339.

744 DeMaster, D.J (2002) C14 ages, sediment cores, EqPac/Cruise TT013, Benthic survey.
745 United States JGOFS Data Server. Woods Hole Oceanographic Institution, USA:
746 U.S. JGOFS Data Management Office, iPub. Accessed: 2013.
747 http://usjgofs.whoi.edu/jg/dir/jgofs/eqpac/tt013/

748 Dubois, L. G., and W. L. Prell (1988), Effects of carbonate dissolution on the radiocarbon
749 age structure of sediment mixed layers. , Deep-Sea Research, 35(12), 1875-1885.

750 Dymond, J., and R. Collier (1988), Biogenic particle fluxes in the equatorial Pacific:
751 Evidence for both high and low productivity during the 1982-1983 El Niño,
752 Global Biogeochemical Cycles, 2(2), 129-139.

753 Dymond, J., E. Suess, and M. Lyle (1992), Barium in deep-sea sediment: A geochemical
754 proxy for paleoproductivity, Paleoceanography, 7(2), 163-181.
755 Dymond, J., and M. Lyle (1994), Particle fluxes in the ocean and implications for sources
756 and preservation of ocean sediments, in Material Fluxes on the Surface of the
757 Earth, edited by W. W. Hay, et al., pp. 125-143, National Academy Press,
758 Washington DC.
759 Dymond, J., and R. Collier (1996), Particulate barium fluxes and their relationships to
760 biological productivity, Deep Sea Research II, 43(4-6), 1283-1308.
761 Dymond, J., R. Collier, and J. McManus (1997), Can the aluminum and titanium contents
762 of ocean sediments be used to determine the paleoproductivity of the oceans?,
763 *Paleoceanography*, *12*(4), 585-593.
764 Emerson, S., V. Grundmanis, and D. Graham (1982), Carbonate chemistry in marine pore
765 waters: MANOP sites C and S, Earth and Planetary Science Letters, 61, 220-232.
766 Farrell, J. W., and W. L. Prell (1989), Climatic change and CaCO3 preservation: an
767 800,000 year bathymetric reconstruction from the central equatorial Pacific
768 Ocean, Paleoceanography, 4(4), 447-466.
769 Farrell, J. W., I. Raffi, T. R. Janecek, D. W. Murray, M. Levitan, K. A. Dadey, K.-C.
770 Emeis, M. Lyle, J.-A. Flores, and S. and Hovan (1995), Late Neogene
771 sedimentation patterns in the eastern equatorial Pacific Ocean, in Proceedings of
772 the Ocean Drilling Program, Scientific Results, edited by N. G. Pisias, L. A.
773 Mayer, T. R. Janecek, A. Palmer-Julson and T. H. van Andel, pp. 717-756, Ocean
774 Drilling Program, College Station, Texas.

775 Francois, R., M. Frank, M. M. Rutgers van der Loeff, and M. P. Bacon (2004), 230Th-
776 normalization: an essential tool for interpreting sedimentary fluxes during the late
777 Quaternary, Paleoceanography, 19, doi:10.1029/2003PA000939.

778 Honjo, S., J. Dymond, R. Collier, and S. J. Manganini (1995), Export production of
779 particles to the interior of the equatorial Pacific Ocean during the 1992 EqPac
780 experiment, Deep-Sea Research, 42(2-3), 831-870.

781 Huh, C.-A., L. F. Small, S. Niemnil, B. P. Finney, B. M. Hickey, N. B. Kachel, D. S.
782 Gorsline, and P. M. Williams (1990), Sedimentation dynamics in the Santa
783 Monica-San Pedro Basin off Los Angeles: radiochemical, sediment trap and
784 transmissometer studies, *Continental Shelf Research*, *10*(2), 137-164.Kennett, J.
785 P. (1982), Marine Geology, 813pp., Prentice-Hall, Englewood Cliffs, N.J.

786 Johnson, G. C., and J. M. Toole (1993), flow of deep and bottom waters in the Pacific at
787 10°N, *Deep Sea Research I*, *40*(2), 371-394.

788 Keir, R. S., and R. L. Michel (1993), Interface dissolution control of the ^{14}C profile in
789 marine sediment, *Geochimica et Cosmochimica Acta*, *57*, 3563-3573.

790 Kretschmer, S., W. Geibert, M. M. Rutgers van der Loeff, and G. Mollenhauer (2010),
791 Grain size effects on 230Thxs inventories in opal-rich and carbonate-rich marine
792 sediments, Earth and Planetary Science Letters, 294, 131-142.

793 Krishnaswami, S. (1976), Authigenic transition elements in Pacific pelagic clays,
794 *Geochimica et Cosmochimica Acta*, *40*, 425-434.

795 Lyle, M., D. W. Murray, B. P. Finney, J. Dymond, J. M. Robbins, and K. Brooksforce
796 (1988), The record of Late Pleistocene biogenic sedimentation in the eastern
797 tropical Pacific Ocean, Paleoceanography, 3, 39-59.

798 Lyle, M., N. C. Mitchell, N. Pisias, A. Mix, J. I. Martinez, and A. Paytan (2005), Do
799 geochemical estimates of sediment focusing pass the sediment test in the
800 equatorial Pacific, *Paleoceanography*, *20*, doi:10.1029/2004PA001019.

801 Mahannah, R. N. (1984) Uranium and thorium series isotopes in sediment trap material
802 from MANOP Sites H and M in the eastern Pacific Ocean. Unpublished MSc
803 thesis, University of South Carolina, 78 pp.

804 Marcantonio, F., R. F. Anderson, M. Stute, N. Kumar, P. Schlosser, and A. Mix (1996),
805 Extraterrestrial 3-He as a tracer of marine sediment transport and accumulation,
806 Nature, 383(24 October), 705-707.

807 Marcantonio, F., R. F. Anderson, S. Higg1ns, M. Stute, P. Schlosser, and P. Kubik
808 (2001), Sediment focusing in the central equatorial Pacific Ocean,
809 Paleoceanography, 16(3), 260-267.

810 Marcantonio, F., M. Lyle, R. Ibrahim (2013) Particle sorting during sediment
811 redistribution processes and the effect on ^{230}Th-normalized mass accumulation
812 rates. 11th International Conference on Paleoceanography, abstracts.

813 McCave, I. N. (1984), Size spectra and aggregation of suspended particles in the deep
814 ocean, *Deep-Sea Research*, *31*(4), 329-352.

815 McCave, I. N. (1986), Local and global aspects of the bottom nepheloid layers in the
816 world ocean, *Netherlands Journal of Sea Research*, *20*(2/3), 167-181.

817 McCave, I. N. (2009), Nepheloid Layers, in *Encyclopedia of Ocean Science, 2nd Edition*,
818 edited by J. H. Steele, editor-in-chief, pp. 1861-1869, Academic Press, Oxford.
819 McGee, D., F. Marcantonio, J. F. McManus, and G. Winckler (2010), The response of
820 excess 230Th and extraterrestrial 3He to sediment redistribution at the Blake
821 Ridge, western North Atlantic, *Earth and Planetary Science Letters*, *299*, 138-
822 149.
823 McManus, J., D. E. Hammond, W. M. Berelson, T. E. Kilgore, D. J. DeMaster, O. G.
824 Ragueneau, and R. W. Collier (1995), Early diagenesis of biogenic opal:
825 dissolution rates, kinetics, and paleoceanographic implications, Deep Sea
826 Research II, 42(2-3), 871-903.
827 Mitchell, N. C., and J. M. Huthnance (2013), Geomorphological and geochemical
828 evidence (^{230}Th anomalies) for cross-equatorial currents in the central Pacific,
829 *Deep Sea Research I*, *178*, 24-14.
830 Moore, T. C., jr., J. Backman, I. Raffi, C. A. Nigrini, A. Sanfilippo, H. Pälike, and M.
831 Lyle (2004), The Paleogene tropical Pacific: clues to circulation, productivity and
832 plate motion, Paleoceanography, 19, doi:10.1029/2003PA000998.
833 Murray, D. W. (1987), Spatial and temporal variations in sediment accumulation in the
834 central tropical Pacific, PhD. thesis, 343 pp pp, Oregon State University,
835 Corvallis.
836 Murray, R. W., M. Leinen, and A. R. Isern (1993), Biogenic flux of Al to sediment in the
837 central equatorial Pacific Ocean: Evidence for increased productivity during
838 glacial periods, Paleoceanography, 8(5), 651-671.

839 Murray, J. W., R. T. Barber, M. R. Roman, M. P. Bacon, and R. A. Feely (1994),
840 Physical and Biological Controls on Carbon Cycling in the Equatorial Pacific,
841 Science, 266, 58-65.

842 Murray, R. W., M. Leinen, D. W. Murray, A. C. Mix, and C. W. Knowlton (1995),
843 Terrigenous Fe input and biogenic sedimentation in the glacial and interglacial
844 equatorial Pacific Ocean, Global Biogeochemical Cycles, 9(4), 667-684.

845 Murray, R. W., and M. Leinen (1996), Scavenged excess aluminum and its relationship
846 to bulk titanium in biogenic sediment from the central equatorial Pacific Ocean,
847 *Geochimica et Cosmochimica Acta*, *60*(20), 3869-3878.

848 Murray, R. W., C. Knowlton, M. Leinen, A. Mix, and C. H. Polsky (2000), Export
849 production and carbonate dissolution in the central equatorial Pacific Ocean over
850 the past 1 Myr, Paleoceanography, 15(6), 570-592.

851 Murray, R. W., M. Leinen, and C. W. Knowlton (2012), Links between iron input and
852 opal deposition in the Pleistocene equatorial Pacific Ocean, *Nature Geoscience*, *5*,
853 270-274.

854 Pares, J. M., and T. C. Moore (2005), New evidence for the Hawaiian Hotspot plume
855 motion since the Eocene, Earth and Planetary Science Letters, 237, 951-959.

856 Paytan, A., M. Kastner, and F. Chavez (1996), Glacial to interglacial fluctuations in
857 productivity in the equatorial Pacific as indicated by marine barite, Science, 214,
858 1355-1357.

Singh, A. K., F. Marcantonio, and M. Lyle (2013), Water column 230Th systematics in the eastern equatorial Pacific Ocean and implications for sediment focusing. , *Earth and Planetary Science Letters*, *362*, 294-304.

Stephens, M. P., and D. C. Kadko (1997), Glacial-Holocene calcium carbonate dissolution at the central equatorial Pacific seafloor, *Paleoceanography*, *12*(6), 797-804.

Suman, D. O., and M. P. Bacon (1989), Variations in Holocene sedimentation in the North American Basin determined from 230Th measurements, Deep-Sea Research, 36(6), 869-878.

Talley, L. D., G. L. Pickard, W. L. Emery, and J. H. Swift (2011), *Descriptive Physical Oceanography: an introduction (6th edition)*, Academic press.

Thomson, J., S. Colley, R. Anderson, G. T. Cook, A. B. MacKenzie, and D. D. Harkness (1993), Holocene sediment fluxes in the northeast Atlantic from 230Thexcess and radiocarbon measurements, Paleoceanography, 8(5), 631-650.

Tominaga, M., M. Lyle, and N. C. Mitchell (2011), Seismic interpretation of pelagic sedimentation regimes in the 18–53 Ma eastern equatorial Pacific: Basin-scale sedimentation and infilling of abyssal valleys, Geochemistry, Geophysics, Geosystems, 12(3), Q03004, 22p.

Turnewitsch, R., S. Falahat, J. Nycander, A. Dale, R. B. Scott, and D. Furnival (2013), Deep-sea fluid and sediment dynamics--influence of hill- to seamoun-scale seafloor topography, *Earth-Science Reviews*, *127*, 203-241.

van Andel, T. H., G. R. Heath, and T. C. j. Moore (1975), Cenozoic History and Paleoceanography of the central equatorial Pacific Ocean, GSA Memoir 143, 133 pp., Geological Society of America.

Walsh, I., K. Fischer, D. Murray, and J. Dymond (1988a), Evidence for resuspension of rebound particles from near-bottom sediment traps, Deep-Sea Research, 35, 59-70.

Walsh, I., J. Dymond, and R. B. Collier (1988b), Rates of recycling of biogenic components of settling particles in the ocean derived from sediment trap experiments, Deep-Sea Research, 35, 43-58.

Winckler, G., R. F. Anderson, M. Q. Fleisher, D. McGee, and N. Mahowald (2008), Covariant glacial-interglacial dust fluxes in the equatorial Pacific and Antarctica., *Science*, *320*, 93-96

Tables:

Table 1: Calculations of Holocene MAR and sediment focusing

Table 2: Sediment trap fluxes, MANOP Site C

Table 3: biogenic fluxes in different size fractions from MANOP Site C sediment traps from Murray (1987)

Table 4: ^{230}Th and Al fluxes in near-bottom sediment traps, modeled from resuspension of surface sediments versus measured

Figure captions

Figure 1. Map of (a) the JGOFS equatorial study site constructed using GeoMapApp (http://www.geomapapp.org/). Available high-resolution multibeam survey data is superimposed over low-resolution satellite-estimated sea floor topography. Cores discussed in the study are shown, along with the location of the 1992 sediment trap deployment. (b) Map of MANOP Site C showing core sites and location of sediment trap moorings. Topography shown was imaged using GeoMapApp (http://www.geomapapp.org/) and shows high-resolution swathmap bathymetry superimposed over satellite-estimated sea floor topography.

Figure 2. Comparison of excess Al MAR (Al MAR/Al particulate rain) compared to the ^{230}Th derived focusing factor (excess ^{230}Th MAR/assumed ^{230}Th rain). If the focusing factor adequately describes lateral sediment transport for Al, the data should lie on the 1:1 line. Al MAR is actually 20% greater than expected by the focusing model.

Figure 3. Comparison of $CaCO_3$ MAR versus the ^{30}Th focusing factor for 2 different MAR models. Heavy black regression line and filled black circles mark 'observed' $CaCO_3$ MAR calculated from sediment age, $CaCO_3$ content, and dry bulk density. Red open squares and the red regression line mark expected $CaCO_3$ MAR from a no-focus model, calculated by subtracting estimated Holocene dissolution from $CaCO_3$ rain

921 measured by sediment traps but assuming no lateral sediment additions. Blue open
922 circles and the blue regression line mark the focused sediment model, where the $CaCO_3$
923 rain is multiplied by the ^{230}Th focusing factor, assuming the focusing factor measures
924 lateral additions of $CaCO_3$. When the focusing factor is high, the focused model
925 significantly overpredicts the $CaCO_3$ MAR that should have been observed.

926

927 Figure 4. a. Deep-tow photograph taken in 1980 on RAMA-1 cruise of the footprint of a
928 box core taken in 1979 on Knorr cruise K7905. b. picture of the box core being launched
929 on a different coring expedition to show the frame of the box core that made the
930 footprint. Where the frame set down on the sea floor is still clearly visible a year later,
931 indicating weak current activity.

932

933 Figure 5. a. Fluxes of ^{230}Th caught in the JGOFS and MANOP Site C sediment trap
934 deployments. Only the MANOP deployment employed sediment traps in the
935 resuspension zone. ^{230}Th fluxes follow a water column production model until about 500
936 m above the bottom. High amounts of ^{230}Th are found in the resuspended sediment near
937 the sea floor. b. ^{230}Th:CaCO3 in the equatorial Pacific sediment trap arrays. High
938 ^{230}Th:CaCO3 in the resuspension zone is evidence that a ^{230}Th-rich fraction is
939 preferentially resuspended as compared to $CaCO_3$. Black dot indicates the expected
940 230Th:CaCO3 following continued water column dissolution of $CaCO_3$ [Walsh et al,
941 1988b].and continued ^{230}Th scavenging as particulate rain falls to the sea floor.

942

Supplemental material

1) Supplemental Table S1 W84-14 ^{230}Th and ^{232}Th from Huh and Finney, chemical data from Murray (1987)
2) Supplemental Table S2: ^{230}Th fluxes JGOFS sediment traps calculated from fluxes in Honjo et al (1995) and ^{230}Th contents measured by Anderson [2002a]
3) Supplemental Table S3: MANOP Site S, M, and H sediment trap data with radiochemical fluxes. Site M and H data from Mahannah (1984)
4) Supplemental Table S4: Radiocarbon measurements in MANOP Site C sediment traps by Alan Mix

Lyle et al, Figure 1: Map of (a) the JGOFS equatorial study site constructed using GeoMapApp (http://www.geomapapp.org/). Available high-resolution multibeam survey data is superimposed over low-resolution satellite-estimated sea floor topography. Cores discussed in the study are shown, along with the location of the 1992 sediment trap deployment.
(b) Map of MANOP Site C showing core sites and location of sediment trap moorings. Topography shown was imaged using GeoMapApp (http://www.geomapapp.org/) and shows high-resolution swathmap bathymetry superimposed over satellite-estimated sea floor topography.

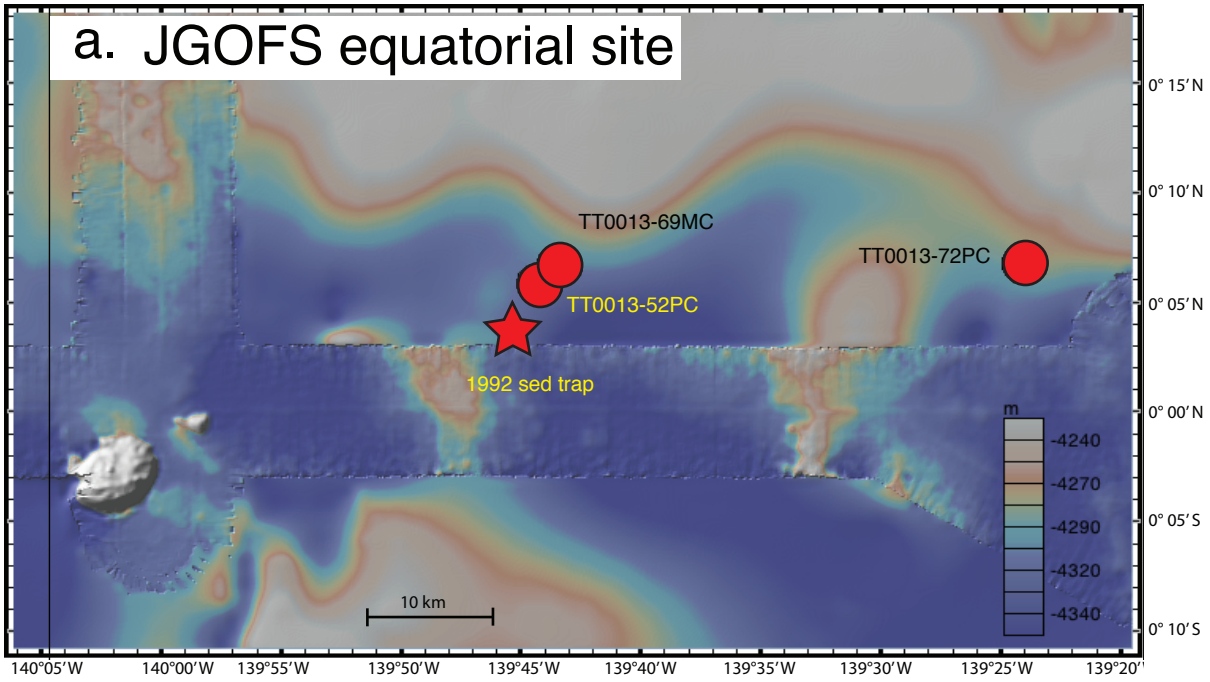

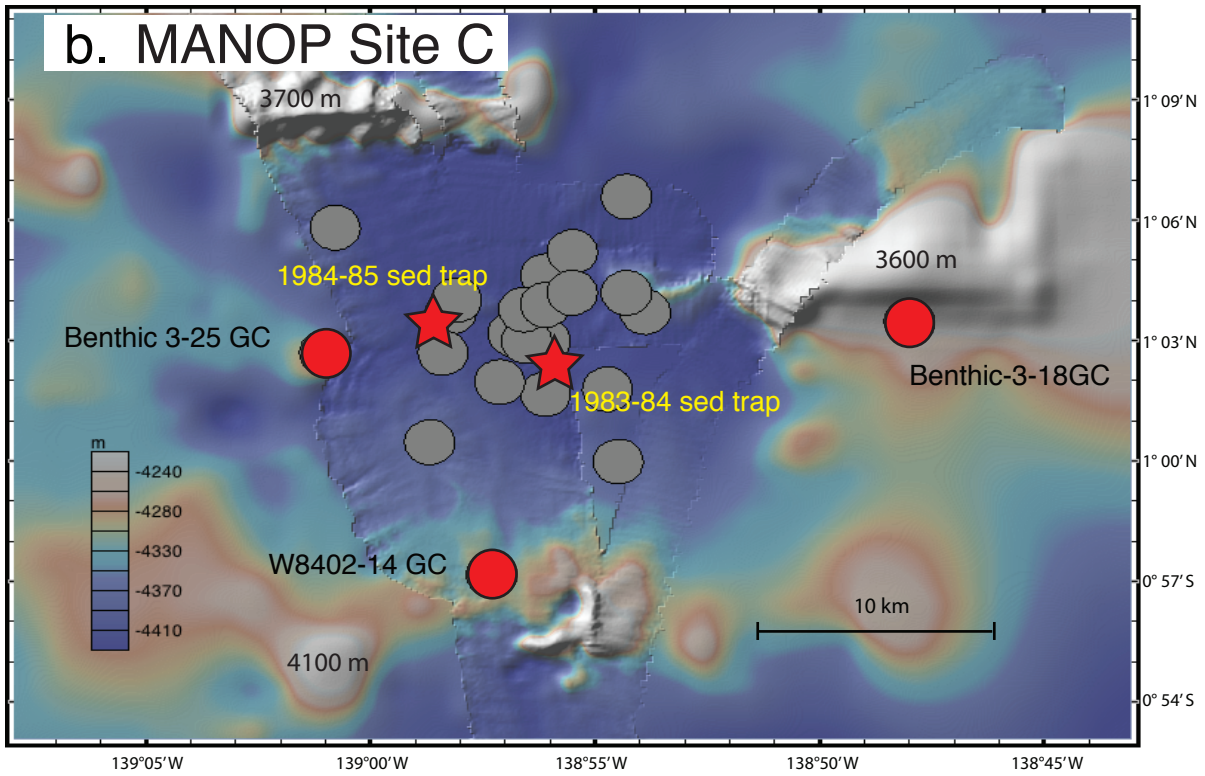

Lyle et al. Figure 2. Comparison of excess Al MAR (Al MAR/Al particulate rain) compared to the 230Th derived focusing factor (excess 230Th MAR/assumed 230Th rain). If the focusing factor adequately describes lateral sediment transport for Al, the data should lie on the 1:1 line. Al MAR is actually 20% greater than expected by the focusing model.

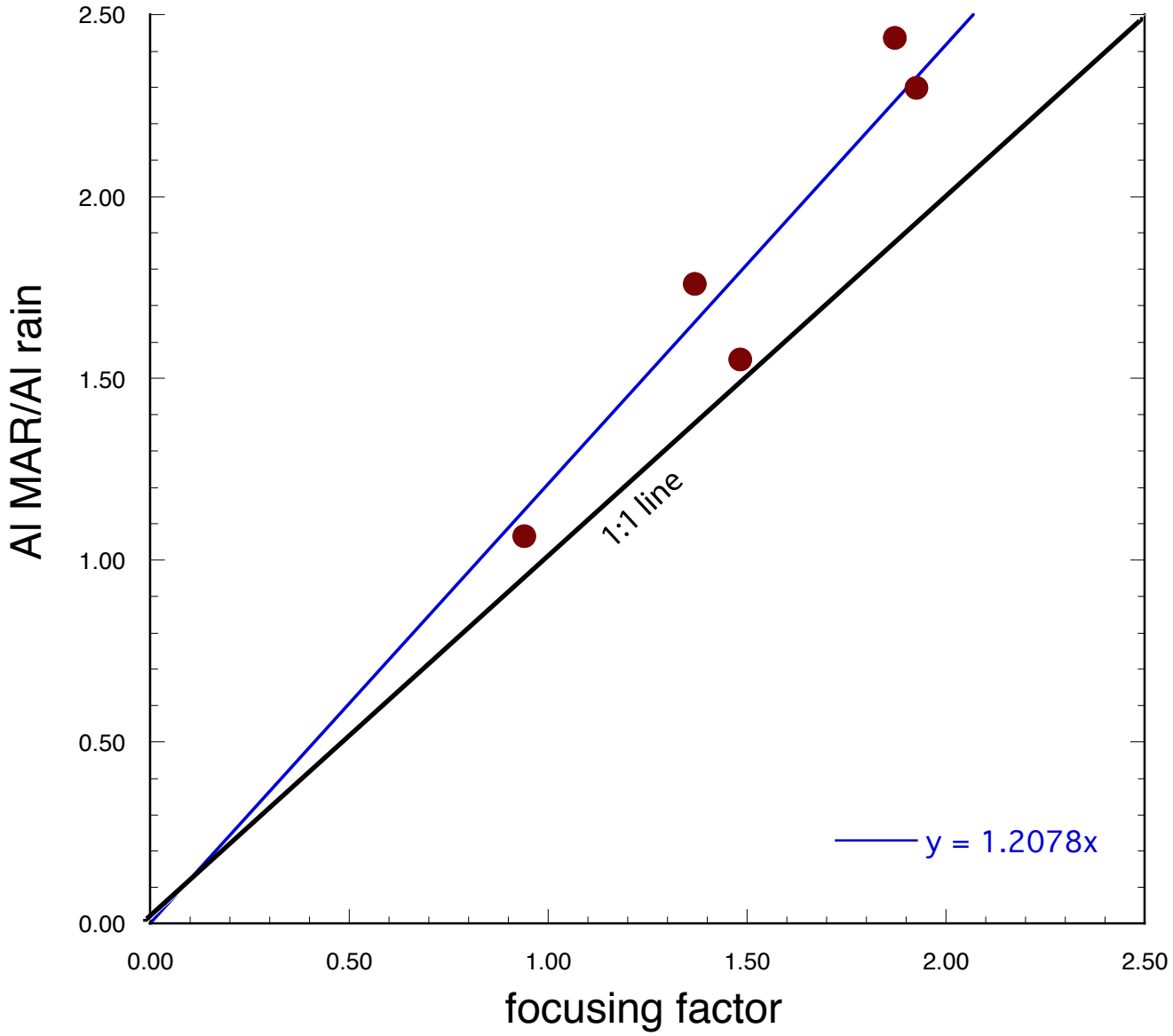

Lyle et al. Figure 3. Comparison of CaCO3 MAR versus the 30Th focusing factor for 2 different MAR models. Heavy black regression line and filled black circles mark 'observed' CaCO3 MAR calculated from sediment age, CaCO3 content, and dry bulk density. Red open squares and the red regression line mark expected CaCO3 MAR from a no-focus model, calculated by subtracting estimated Holocene dissolution from CaCO3 rain measured by sediment traps but assuming no lateral sediment additions. Blue open circles and the blue regression line mark the focused sediment model, where the CaCO3 rain is multiplied by the 230Th focusing factor, assuming the focusing factor measures lateral additions of CaCO3. When the focusing factor is high, the focused model significantly overpredicts the CaCO3 MAR that should have been observed.

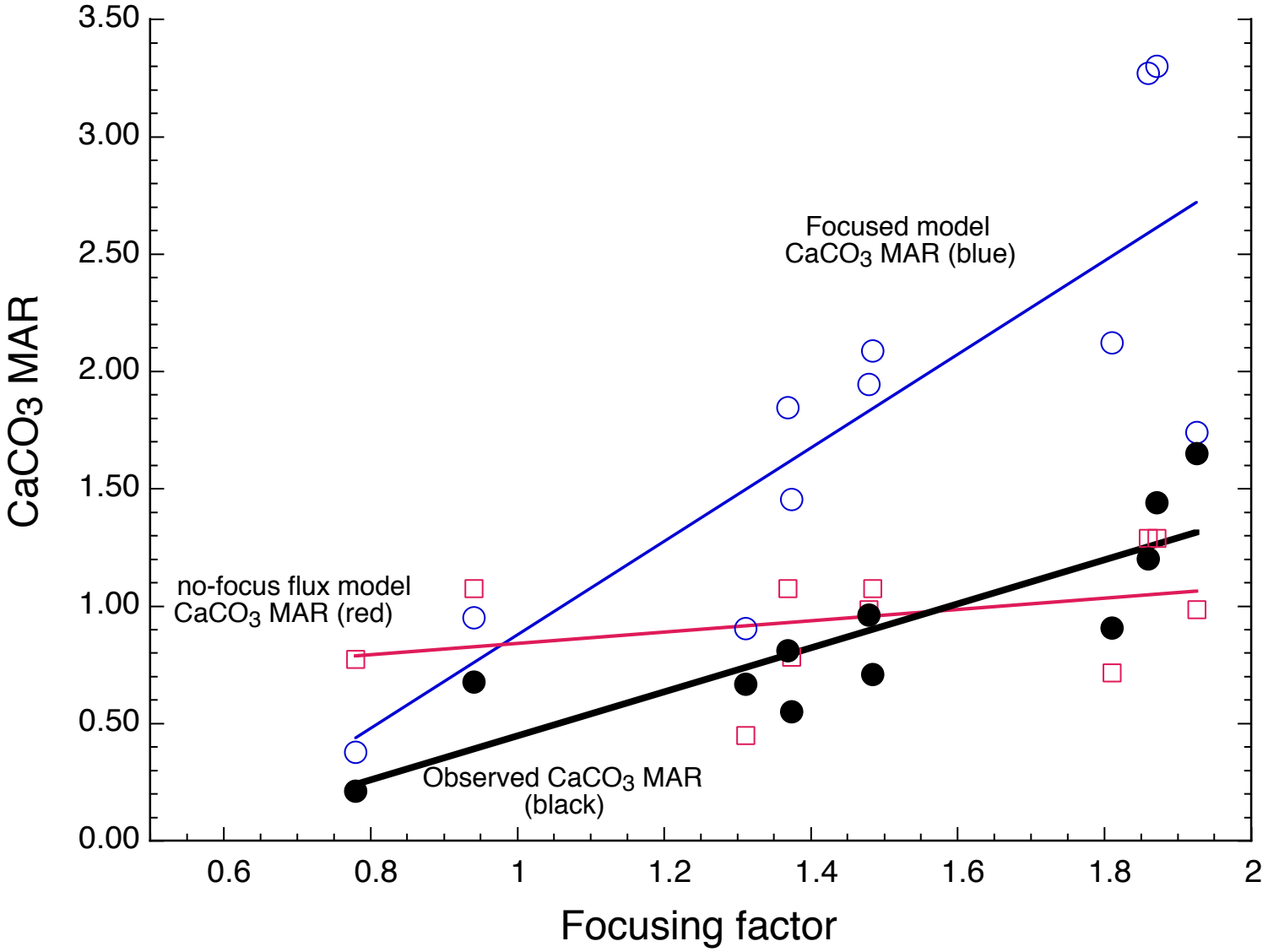

Lyle et al. Figure 4. a. Deep-tow photograph taken in 1980 on RAMA-1 of the footprint of a box core taken in 1979 on Knorr cruise K7905. b. picture of the box core being launched on a different coring expedition to show the frame of the box core that made the footprint. Where the frame set down on the sea floor is still clearly visible a year later, indicating weak current activity.

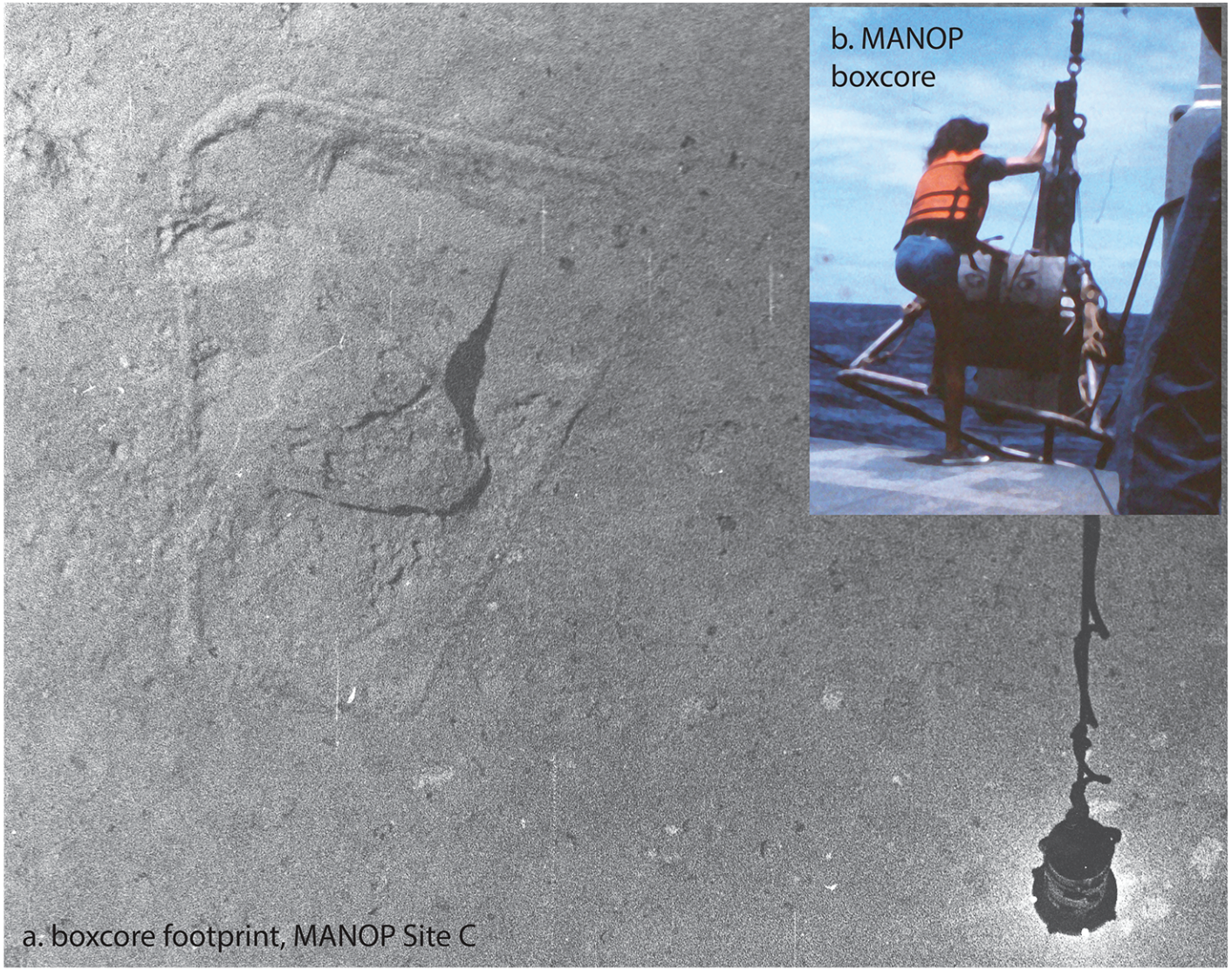

Lyle et al, Figure 4

Lyle et al. Figure 5. Figure 5. a. Fluxes of 230Th caught in the JGOFS and MANOP Site C sediment trap deployments. Only the MANOP deployment employed sediment traps in the resuspension zone. 230Th fluxes follow a water column production model until about 500 m above the bottom. High amounts of 230Th are found in the resuspended sediment near the sea floor. b. 230Th:CaCO3 in the equatorial Pacific sediment trap arrays. High 230Th:CaCO3 in the resuspension zone is evidence that a 230Th-rich fraction is preferentially resuspended as compared to CaCO3. Black dot indicates the expected 230Th:CaCO3 following continued water column dissolution of CaCO3 [Walsh et al, 1988b].and continued 230Th scavenging as particulate rain falls to the sea floor.

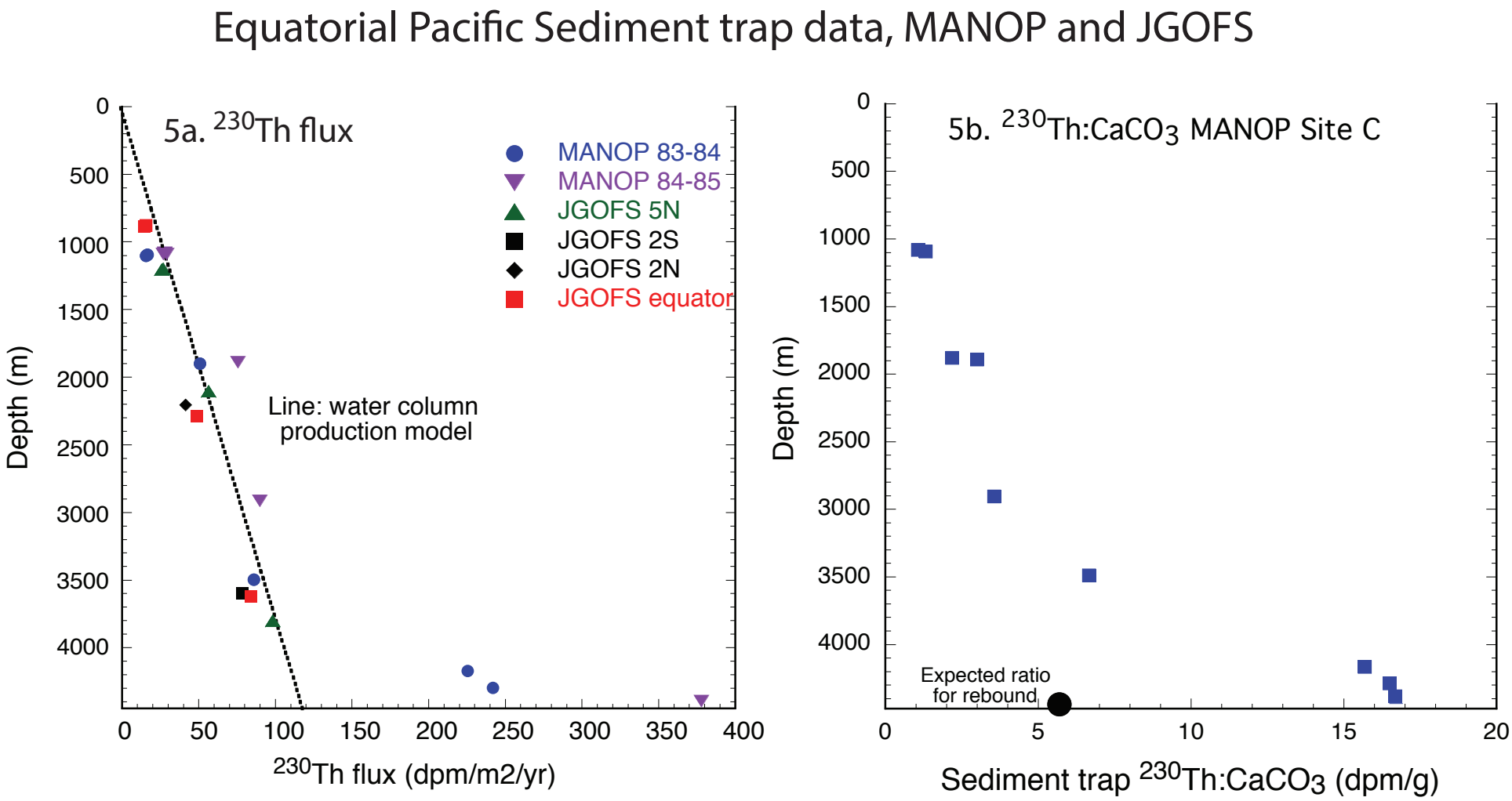

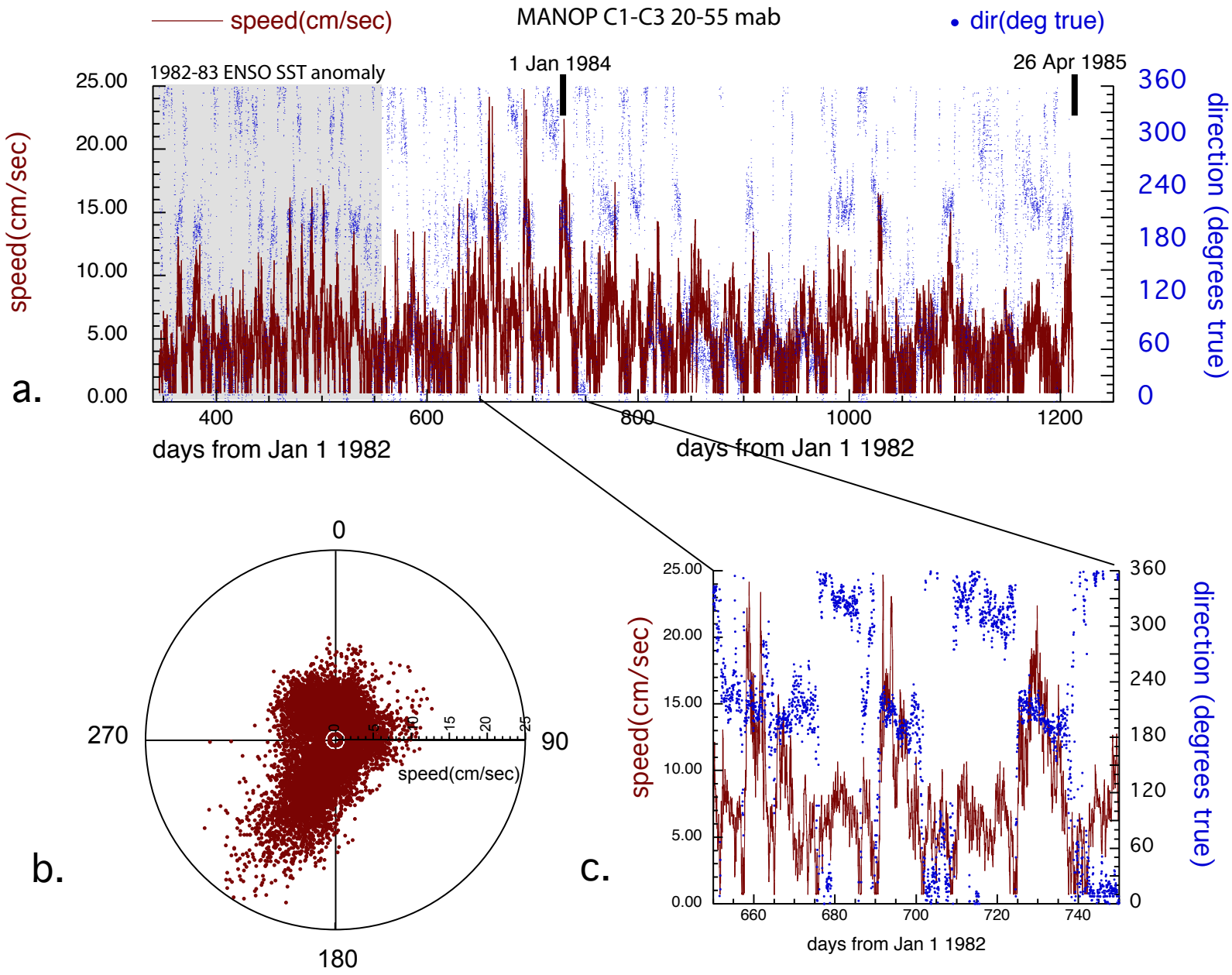

Figure 6. Long-term near-bottom current meter records from MANOP Site C (Table S6). (a) Full 2.37 year records from C-1 and C-3 moorings (data from http://kepler.oce.orst.edu/quick/archive.htm). (b) Current vectors for deployment, showing strongest currents flowing along a SW-NE. (c) Expanded section during the highest current interval showing that high current periods (>15 cm/s) last for as long as 3 days.

Table 1. Calculations of Holocene Mass Accumulation Rates (MAR) and sediment focusing*

Core name	Latitude	Longitude	water depth	ave Holocene XS 230Th dpm/g	Th-230 water column production dpm/cm2/kyr	focusing factor	Average Holocene CaCO3 dissolution g/cm2/kyr	Sediment Trap CaCO3 rain g/cm2/kyr	focussed CaCO3 rain (CaCO3 rain * focusing factor)	Sediment Trap Al rain mg/cm2/kyr	focussed Al rain (Al rain * focusing factor	estimated dry bulk density (g/cm3)	sedimentation rate (cm/kyr)	ave CaCO3% (0-10 ka interval)	average Al% (0-10 ka interval)	Th-230 MAR dpm/cm2/kyr	Al MAR mg/cm2/kyr	Observed Holocene CaCO3 MAR g/cm2/kyr	Focused model CaCO3 MAR (Th-focus rain - Holocene dissolution)	No-focus model CaCO3 MAR (no focusing: rain - holocene dissolution)	Data Sources
TT013-MC34	-4.9738	-139.7373	4256	19.57	11.36352	1.31	1.02	1.467	1.92	0.60		0.754	1.01	87.7		14.903		**0.668**	**0.91**	**0.449**	Anderson et al (2008) for age, Th230; Berelson and Hammond (2002) for dbd from porosity
TT013-MC27	-2.885	-139.832	4513	20.28	12.04971	1.81	1.02	1.735	3.14			0.681	1.58	84.4		21.821		**0.908**	**2.12**	**0.717**	Demaster (2002) radiocarbon age @16 cm rad data and carbonate from Anderson (2002b)
TT013-MC19	-1.868	-139.7157	4376	14.82	11.68392	1.48	1.02	2.003	2.96	1.46		0.659	1.77	82.6		17.286		**0.963**	**1.95**	**0.985**	sed rate from radiocarbon on Anderson (2002b), using Calib 6; dbd Berelson and Hammond (2002) porosity; CaCO3 rain is average of 5 and 2 S rain
TT013-PC18	-1.8395	-139.7137	4354	11.88	11.62518	1.93	1.02	2.003	3.86	1.46	2.81	0.809	2.33	87.5	0.1787	22.393	3.37	**1.649**	**2.84**	**0.985**	Murray et al, (2000) sed rate from 10.5 ka to top sample; Some data with Anderson et al 2006--Holocene in JGOFS data library
TT013-MC69	0.112	-139.723	4440	15.23	11.8548	1.86	1.02	2.307	4.29	1.65		0.720	2.01	83		22.048		**1.202**	**3.27**	**1.289**	sed rate Anderson (2002b) radiocarbon
TT013-PC72	0.114	-139.402	4298	12.49	11.47566	1.87	1.02	2.307	4.32	1.65	3.09	0.735	2.34	83.8	0.2328	21.482	4.02	**1.441**	**3.30**	**1.289**	Marcantonio(1995):radion uclides; Murray et al (2000) age model
W8402-14 GC	0.953	-138.955	4287	16.29	11.44629	1.37	1.02	2.093	2.86	2.41	3.30	0.569	1.69	84.2	0.4407	15.665	4.24	**0.810**	**1.85**	**1.075**	Murray (1987) age model; radionuclides this paper
Benthic 25BC	1.045	-139.017	4401	19.05	11.75067	1.48	1.02	2.093	3.11	2.41	3.58	0.601	1.52	77.5	0.4094	17.437	3.74	**0.709**	**2.09**	**1.075**	Marcantonio et al (2001) radionuclides; Murray (1987) dbd, CaCO3, and age model
Benthic 18BC	1.058	-138.8	4281	13.36	11.43027	0.94	1.02	2.093	1.97	2.41	2.27	0.639	1.26	84.1	0.3207	10.757	2.57	**0.677**	**0.95**	**1.075**	Marcantonio et al (2001) radionuclides; Murray (1987) dbd, CaCO3, and age model
TT013-MC97	2.05	-140.143	4540	24.6	12.1218	1.37	1.02	1.800	2.47	1.03		0.594	1.14	81.2		16.658		**0.550**	**1.46**	**0.782**	Radiocarbon: Anderson et al (2008); radionuclides and CaCO3: Anderson (2002b)
TT013-MC112	5.0783	-139.6383	4418	35.94	11.79606	0.78	1.02	1.792	1.40	1.38		0.599	0.43	82.8		9.192		**0.212**	**0.38**	**0.774**	Radiocarbon: Anderson et al (2008); radionuclides and CaCO3: Anderson (2002b; dbd: Berelson and Hammond (2002) porosity fo stn108 used for dbd

*CaCO3 and Al particulate rain data from Honjo et al (1995) and Table 2

Table 2. Sediment trap fluxes, MANOP Site C deployments*

Sample	Depth	Cup	days open	cup open date	cup close date	Mass Flux	Th-232	Th-230	Th-228	Pa-231	Al	Organic Carbon	Opal	Al flux	C-org flux	opal flux	CaCO3 flux	Th-230 Flux	Pa-231 Flux	Th-230/Al	Th-230/CaCO3
	meters			days from 1/1/1982)	days from 1/1/1982)	mg/cm2-yr	dpm/gm	dpm/gm	dpm/gm	dpm/gm	µM/gm	mM/gm	mg/gm	mg/cm2/yr	mg/cm2/yr	mg/cm2/yr	mg/cm 2/yr	dpm/m2-yr	dpm/m2-yr	dpm/mg	dpm/g
1983-84 C-1 and C-2 moorings																					
C-2																					
22929	1095	2	100	352	452	1.38	0.00	1.02	4.98	0.00	15.91	5.17	119	0.000592	0.0857	0.1640	0.954	14.0	0.0	2.37	1.47
22930	1095	3	100	452	552	1.37	0.00	0.94	3.59	0.00	15.54	5.96	206	0.000574	0.0981	0.2820	0.853	12.8	0.0	2.23	1.50
22931	1095	4	100	552	652	2.54	0.00	1.09	5.05	0.00	29.60	5.28	396	0.002028	0.1610	1.0060	1.153	27.8	0.0	1.37	2.41
22932	1095	5	128	652	780	1.64	0.00	0.78	2.93	0.00	21.09	4.71	391	0.000933	0.0926	0.6420	0.907	12.8	0.0	1.38	1.42
average			**428**			**1.73**	**0.00**	**0.95**	**4.06**	**0.00**				**0.001026**	**0.1082**	**0.5313**	**0.963**	**16.60**	**0.00**	**1.62**	**1.72**
C-2																					
22933	1895	2	100	352	452	1.90	0.00	1.90	2.40	0.00	18.13	4.08	185	0.000929	0.0931	0.3510	1.330	36.2	0.0	3.89	2.72
22934	1895	3	100	452	552	2.48	0.00	1.90	3.89	0.00	25.53	5.67	229	0.001708	0.1688	0.5670	1.581	47.0	0.0	2.75	2.97
22935	1895	4	100	552	652	3.01	0.02	2.01	5.56	0.00	31.82	5.34	408	0.002584	0.1929	1.2280	1.573	60.6	0.0	2.35	3.85
22936	1895	5	128	652	780	3.22	0.01	1.87	3.80	0.12	31.82	4.22	437	0.002764	0.1632	1.4060	1.579	60.2	3.7	2.18	3.81
average			**428**			**2.69**	**0.01**	**1.92**	**3.90**	**0.03**				**0.002047**	**0.1551**	**0.9219**	**1.520**	**51.60**	**1.12**	**2.52**	**3.39**
C-2																					
22939	3495	2	100	352	452	1.87	0.03	4.96	3.09	0.37	24.79	3.87	216	0.001251	0.0867	0.4030	1.265	92.7	6.9	7.41	7.33
22940	3495	3	100	452	552	2.36	0.01	4.45	3.83	0.21	23.68	4.69	260	0.001508	0.1328	0.6130	1.473	105.0	5.1	6.97	7.13
22941	3495	4	100	552	652	2.83	0.03	4.09	4.68	0.27	37.00	5.27	382	0.002825	0.1791	1.0820	1.362	115.7	7.6	4.10	8.49
22942	3495	5	128	652	780	1.76	0.04	2.60	3.26	0.19	36.63	4.08	397	0.001739	0.0862	0.6980	0.912	45.7	3.3	2.63	5.01
average			**428**			**2.18**	**0.03**	**3.93**	**3.68**	**0.25**				**0.001825**	**0.1189**	**0.6989**	**1.231**	**86.90**	**5.55**	**4.76**	**7.06**
C-1																					
22919	4170	2	100	352	452	1.99	0.05	8.51	5.16	0.48	52.54	3.60	246	0.002821	0.0859	0.4897	1.291	169.4	9.6	6.01	13.13
22920	4170	3	100	452	552	2.41	0.05	8.37	5.75	0.47	51.80	3.85	233	0.003368	0.1113	0.5615	1.483	201.6	11.3	5.99	13.60
22921	4170	4	100	552	652	2.92	0.03	8.42	7.29	0.39	58.09	4.00	371	0.004576	0.1401	1.0830	1.359	245.8	11.4	5.37	18.09
22922	4170	5	128	652	780	3.00	0.05	9.11	5.25	0.66	71.41	3.27	349	0.005780	0.1179	1.0461	1.579	273.4	19.9	4.73	17.31
average			**428**			**2.61**	**0.05**	**8.64**	**5.82**	**0.51**				**0.004244**	**0.1141**	**0.8115**	**1.439**	**225.89**	**13.49**	**5.32**	**15.70**
C-1																					
22925	4295	2	100	352	452	3.07	0.05	9.59	8.42	0.46	72.15	3.14	336	0.005976	0.1157	1.0327	1.551	294.4	14.2	4.93	18.99
22924	4295	3	100	452	552	2.76	0.04	9.14	5.95	0.42	55.87	4.14	225	0.004160	0.1371	0.6210	1.713	252.2	11.6	6.06	14.72
22923	4295	4	100	552	652	2.42	0.05	10.05	4.85	0.39	58.46	4.90	236	0.003817	0.1422	0.5718	1.487	243.2	9.4	6.37	16.35
22943	4295	5	128	652	780	2.32	0.05	8.35	5.84	0.38	60.31	3.92	351	0.003775	0.1092	0.8132	1.204	193.7	8.7	5.13	16.09
average			**428**			**2.62**	**0.05**	**9.22**	**6.24**	**0.41**				**0.004389**	**0.1250**	**0.7632**	**1.468**	**242.49**	**10.83**	**5.52**	**16.52**
1984-85 C-3 moorings																					
25033	1083	2	36	786	822	2.25	0.00	1.16	3.42	0.14	24.05	4.46	322	0.001460	0.1206	0.7250	1.299	26.1	3.1	1.79	2.01
25034	1083	3	100	822	922	4.63	0.00	1.17	4.29	0.09	18.50	5.70	375	0.002311	0.3166	1.7370	2.532	54.0	4.3	2.34	2.13
25035	1083	4	100	922	1022	4.92	0.00	0.87	2.93	0.10	22.94	4.54	381	0.003045	0.2680	1.8740	2.745	42.9	5.1	1.41	1.56
25036	1083	5	127	1022	1149	2.74	0.01	0.41	2.26	0.07	16.65	3.62	303	0.001231	0.1191	0.8300	1.734	11.3	1.8	0.92	0.65
25032	1083	1	71	1149	1220	2.24	0.00	0.65	1.94	0.08	17.76	3.67	346	0.001073	0.0985	0.7740	1.305	14.5	1.7	1.35	1.11
average			**434**			**3.56**	**0.00**	**0.79**	**2.93**	**0.09**	**19.32**			**0.001891**	**0.1957**	**1.2617**	**2.045**	**30.17**	**2.98**	**1.60**	**1.48**
25038	1883	2	36	786	822	4.63	0.01	1.78	2.99	0.11	35.52	4.54	424	0.004437	0.2522	1.9630	2.267	82.2	5.3	1.85	3.63
25039	1883	3	100	822	922	7.63	0.01	1.49	2.80	0.12	30.34	4.95	375	0.006246	0.4530	2.8610	3.974	113.5	9.1	1.82	2.86
25040	1883	4	100	922	1022	4.81	0.01	1.33	2.39	0.09	23.31	3.41	342	0.003025	0.1967	1.6450	2.817	63.8	4.1	2.11	2.26
25041	1883	5	127	1022	1149	4.87	0.01	1.39	2.75	0.07	24.42	2.87	385	0.003209	0.1675	1.8730	2.742	67.9	3.5	2.12	2.48
25037	1883	1	71	1149	1220	4.67	0.02	1.18	1.97	0.15	24.05	3.01	395	0.003030	0.1685	1.8440	2.508	55.2	6.9	1.82	2.20
average			**434**			**5.44**	**0.01**	**1.40**	**2.57**	**0.10**	**26.39**			**0.003939**	**0.2472**	**2.0508**	**2.965**	**76.58**	**5.24**	**1.94**	**2.58**
25043	2908	2	36	786	822	3.75	0.02	2.81	2.71	0.16	36.26	4.20	389	0.003669	0.1889	1.4600	1.930	105.2	6.1	2.87	5.45
25044	2908	3	100	822	922	3.04	0.05	2.32	2.84	0.14	28.49	4.50	384	0.002337	0.1641	1.1680	1.491	70.6	4.2	3.02	4.73
25045	2908	4	100	922	1022	6.80	0.02	2.31	2.70	0.20	28.86	3.97	355	0.005295	0.3242	2.4130	3.855	157.1	13.8	2.97	4.07
25046	2908	5	127	1022	1149	3.19	0.01	1.82	2.30		21.83	2.92	366	0.001879	0.1116	1.1670	1.894	58.1		3.09	3.07
25042	2908	1	71	1149	1220	4.05	0.02	1.90	2.40	0.14	22.94	3.56	417	0.002507	0.1729	1.6890	2.128	77.1	5.8	3.07	3.62
average			**434**			**4.17**	**0.02**	**2.14**	**2.57**		**26.36**			**0.003023**	**0.1891**	**1.5640**	**2.294**	**90.78**	**5.13**	**3.00**	**3.96**
25053	4390	2	100	786	886	4.34	0.07	10.41	3.74	0.58	79.92	3.58	339	0.009358	0.1865	1.4713	2.311	451.8	25.3	4.83	19.55
25054	4390	3	100	886	986	6.18	0.05	9.80	4.10	0.46	71.04	4.14	344	0.011845	0.3070	2.1253	3.286	605.8	28.1	5.11	18.44
25055	4390	4&5	198	986	1184	3.31	0.03	6.83	4.35	0.36	54.76	3.01	326	0.004890	0.1194	1.0777	1.906	225.9	11.8	4.62	11.85
average			**398**			**4.29**	**0.05**	**8.47**	**4.14**	**0.44**	**65.17**			**0.007760**	**0.1834**	**1.4398**	**2.262**	**378.13**	**19.31**	**4.87**	**16.72**

* C-1 mooring water depth 4470; C-2 mooring water depth 4445; C-3 water depth 4450; expected Th-230 flux at sea floor: 118.8 dpm/m2/yr

Table 3: biogenic fluxes (in mg/cm2/yr) for different size fractions from MANOP Site C sediment traps from Murray (1987)

	<38μ	38-63μ	63-150μ	>150μ	total
CaCO3					
1983-85 trap average	599	116	306	845	1866
1984-85 trap average	532	201	428	1167	2328
W8402-14 surface sediment flux	374	64	155	137	730
Opal					
1983-85 trap average	781	101	129	175	1186
1984-85 trap average	901	152	157	258	1468
W8402-14 surface sediment flux	55	18	37	9.1	119
Residual					
1983-85 trap average	182	52.5	65.9	168	468
1984-85 trap average	53	126	103	265	547
W8402-14 surface sediment flux	52	3.3	6.9	1.8	64

Notes:

The 1983-1985 period includes the 1983-84 ENSO event, while 1984-85 is the post-ENSO period.

1983-85 is a time weighted average of cups 2-4 at 3495 m, cup 5 at 1895 m in the C-1 deployment, and cups 2-5 from 2908 m in C-3

1984-85 is a time weighted average of cups 2-5 from 2908 m in the second deployment (post-1983 ENSO event)

Table 4.Th-230 and Al fluxes in near-bottom sediment traps, modeled from resuspension of surface sediments versus measured

Trap	deployment year	Trap depth	Total Al flux microg/cm2/yr	excess Al flux microg/cm2/yr	%Al resuspended	est 230 Th flux, based on Al resuspension dpm/m2/yr	measured 230 Th flux dpm/m2/yr	excess Th-230 flux (dpm/m2/yr)	CaCO3 flux measured mg/cm2/yr	Walsh et al est primary flux	Excess CaCO3 flux (measured-primary)	% CaCO3 resuspended
C-2 3495	1983	3495	1.83	0.00	0	93	87	-6	1.23		0.00	0
C-1 4170	1983	4170	4.24	2.34	55	209	226	17	1.44	1.18	0.26	18
C-1 4295	1983	4295	4.39	2.49	57	218	242	25	1.47	1.17	0.30	20
C-3 2908	1984	2908	3.02	0.00	0	78	82	4	2.29	2.29		0
C-3 4390	1984	4390	7.76	4.36	56	298	378	80	2.26	2.09	0.17	8

notes:

Excess Al is flux > 1.9 (ave of 1800 &3k traps) year 1; 3.4 (ave of 1800 &3k traps) year 2

ratio for sediment resuspension: Th230/Al of 4.15 dpm/mg Al

use for sed resuspension, CaCO3/Al of 164.8

primary CaCO3 flux is corrected for dissolution using Site C rate constants from Walsh et al (1988b)